Master's Thesis in Physics

Cold Strontium Atoms Coupled to an Optical Cavity

Maria S. V. Larsen

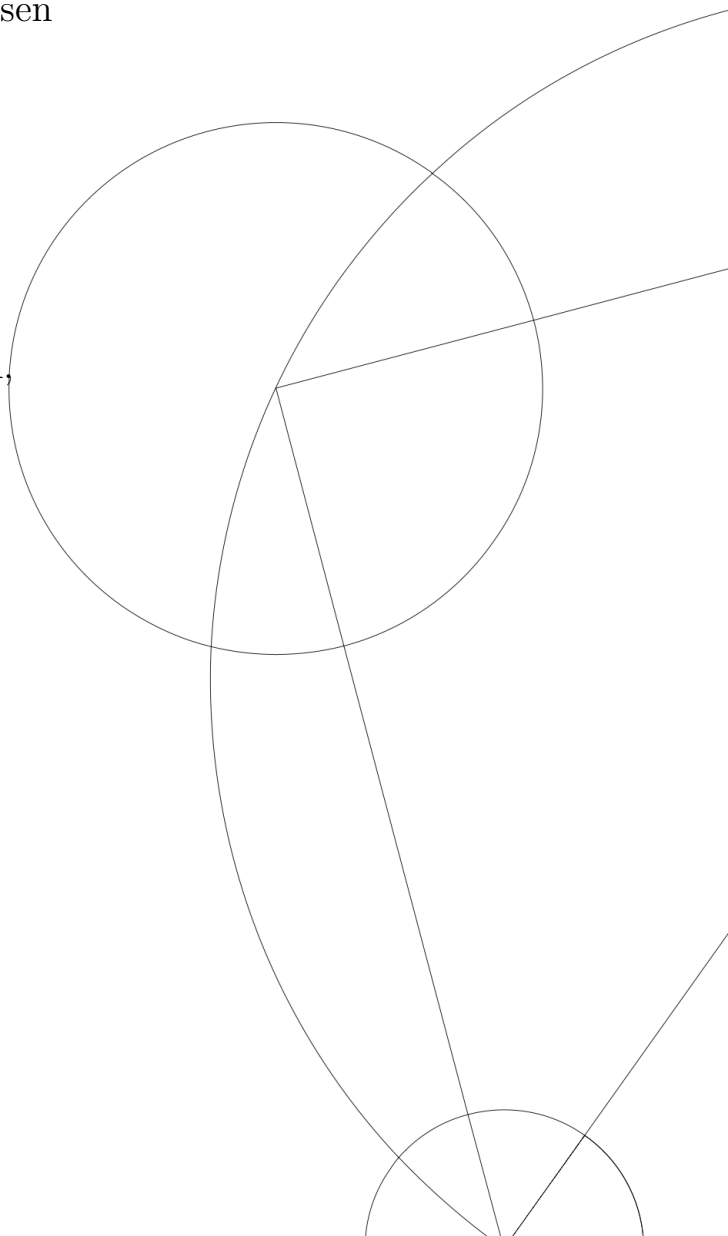

Supervisors
Stefan A. Schäffer, Sofus L. Kristensen,
Mikkel Tang, Jörg H. Müller,
and Jan W. Thomsen

Niels Bohr Institute
29th of November, 2020

Acknowledgements

This thesis work was carried out at the Quantum Metrology group at the Niels Bohr Institute, and many people helped me during this process.

Firstly I would like to thank Jan W. Thomsen for supervising the project. Even though Jan is very busy as head of institute he still took the time to give me feedback during our group meetings, and his enthusiasm for physics is truly contagious. During the second half of my thesis project Jörg H. Müller was the primary supervisor of this project and was a tremendous help with interpreting the experimental results.

My daily supervisors include Sofus L. Kristensen who helped me with the setup for the normal-mode splitting measurements, Stefan A. Schäffer who helped me with the measurements of superradiant pulses, and Mikkel Tang who helped me with the red MOT setup. I am grateful to all of them for their expertise and patience when answering my many questions.

I want to thank my fellow master's students in the Quantum Metrology group: Mantas, Isabella, and Caroline. I enjoyed the many conversations I have had with Caroline - about physics and everything else - and with the rest of my office mates, Anton, Bastian, and Lasse. I had a great time at the "office of the year."

I would also like to thank everyone else in the Quantum Metrology group: Martin, Asbjørn, Eliot, Valentin, and Julian. Thank you all for your contributions to this project during our group meetings and for your help in the lab. For contributions which greatly improved this text I want to thank Sofus, Mikkel and Jörg.

I am grateful for my family and their support and encouragement during my thesis project and all of my physics education. Thank you dad, Jakob and Benjamin - and a huge thanks to my amazing mom for bringing food and snacks for me during the writing process.

Lastly, I want to thank my incredible boyfriend Emil. Your love and support has been invaluable, and your willingness to do all the household chores during the last months of my project allowed me to focus on writing this thesis. Thank you for always being there for me.

Abstract

Atomic clocks are the most stable frequency references and state-of-the-art atomic clocks are limited by thermal fluctuations in the reference cavity mirrors. Superradiant optical clocks where atoms in a cavity emit collectively are advantageous as they lie in the bad-cavity regime and are thus insensitive to noise in the cavity mirrors.

In this work we investigate the theory behind and present a plan for realizing a so-called narrow second-stage magneto-optical trap using the SWAP (Saw-tooth Wave Adiabatic Passage) scheme that cools strontium atoms to the µK level. Cooling the atoms to the µK level level will reduce their Doppler broadening by a factor of 30 thereby bringing the system deeper into the bad-cavity regime.

Furthermore we investigate whether we can achieve closely spaced superradiant lasing pulses by pumping the atoms at short intervals. This is desirable as it means a reduction of the dead time in the experiment, but we found that this was not possible as the excited atoms need to decay between pump pulses.

An important quantity needed to characterize the MOT is the atom number, and in this work we investigate whether we can determine the atom number from the normal-mode splitting of the coupled atom-cavity system. We present measurements of the normal-mode splitting and use the Jaynes-Cummings model to find the atom number in the MOT, yielding a result of $N = (413.08 \pm 0.07) \cdot 10^6$. However, we find that this number overestimates the atom number when compared to the result we obtain from absorption imaging measurements, $N = (129.1 \pm 0.8) \cdot 10^6$. However we found that the normal-mode splitting is insensitive to a range of probe powers meaning we can use it as a proxy for the total atom number.

Nomenclature

AOM	- Acousto-optic modulator
EOM	- Electro-optic modulator
FSR	- Free spectral range
FWHM	- Full width at half maximum
MOT	- Magneto-optical trap
NMS	- Normal-mode splitting
PBS	- Polarizing beam splitter
RF	- Radio frequency
TA	- Tapered amplifier

Contents

List of Figures

List of Tables

CHAPTER 1

Introduction

The ability to precisely determine time is important in technology as well as in fundamental research and relies on stable frequency standards. Frequency standards can be characterized by their accuracy and their stability, and these terms are illustrated in Figure 1.1 as bullet holes on target. The center of the target corresponds to the desired frequency of the frequency standard, and the distance between the bullet holes corresponds to the deviation from the desired frequency. The most accurate frequency standards are atomic clocks and using atomic clocks fractional uncertainties of 10^{-17} [1] have been achieved.

Atomic clocks are used anywhere from GPS satellites to fundamental research. The unit of the second is defined from measurements of the hyperfine electronic transition in cesium-133. This frequency lies in the microwave regime, but as optical frequencies are orders of magnitude larger than microwave frequencies, using optical frequencies is advantageous in terms of reducing fractional frequency uncertainty.

An illustration of the basic components of an atomic clock can be seen in Figure 1.2, where a laser oscillating at frequency f with frequency noise δf is stabilized to an ultra stable reference cavity reducing the noise δf and then sent through an ensemble of atoms with resonance frequency f_0. The resonance frequency of the atoms provide a reference frequency and can be used to correct the laser frequency using a feedback system.

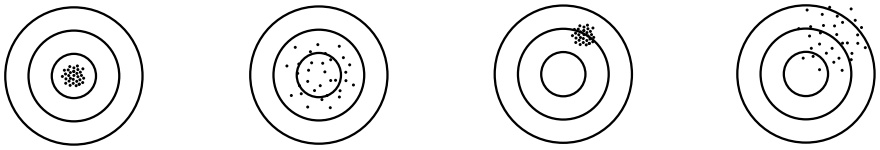

(a) *Precise and accurate.* (b) *Accurate but not precise.* (c) *Precise but not accurate.* (d) *Not precise and not accurate.*

Figure 1.1: *Illustration of the terms accuracy and precision using a target with bullet holes.*

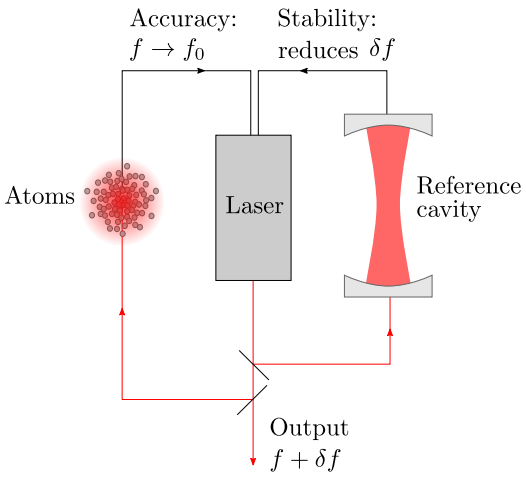

Figure 1.2: *Schematic of the basic components of an optical clock. A laser with frequency f is stabilized to a reference cavity, which reduces the noise, δf, in the laser frequency. The laser light is then corrected using an ensemble of atoms.*

The advantage of using atoms is that atoms of the same species are identical anywhere in the universe, meaning that the control of the environment is the limiting factor in the performance of the frequency reference. One approach to control the atoms is to trap them using a magneto-optical trap (MOT) localized in the center of an optical cavity, an arrangement of mirrors that can greatly enhance the coupling between the atoms and the laser.

We distinguish between two different types of optical clocks: Passive and active. The passive optical clock utilizes the method explained above and shown in Figure 1.2. In an active atomic clock, the interrogation light itself is generated by atoms lasing within an optical cavity, thus eliminating the need for a separate reference laser. This is advantageous as the reference laser needs to be stabilized to a reference cavity, and thus its noise depends on fluctuations in the cavity length, which limits the precision. We wish to operate in the so-called bad-cavity regime, where the coupling to the cavity enables superradiant lasing, meaning the atoms collectively emit light into the cavity mode.

1.1 Superradiant lasers

A typical laser consists of a gain medium and an enhancement cavity. The gain medium amplifies the light via stimulated emission and the cavity mirrors reflects the light leading to repeated interactions with the medium. For traditional laser, the linewidth of the cavity, γ, is narrow compared to the linewidth of the cavity, κ. This so-called good cavity regime, where $\kappa \ll \gamma$, leads to the frequency noise of the laser being dominated by fluctuations in the cavity length. On the other hand, a superradiant laser consists of a gain

medium with narrow linewidth and a cavity with a broad linewidth, the so-called bad-cavity regime where $\kappa \gg \gamma$. Since the gain medium is spectrally narrow, it is the gain medium that dictates the frequency of the lasing, and thus the resulting spectrum is not as affected by fluctuations in the cavity length. A comparison of the good and bad cavity regimes can be seen in Figure 1.3.

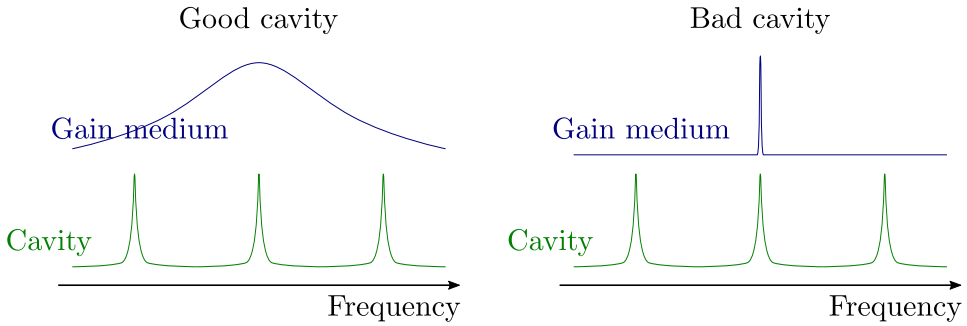

Figure 1.3: *Illustration of the good and bad cavity regimes.*

1.2 The Strontium Clock Experiment

An overview of the experimental setup can be seen in Figure 1.4. A strontium sample is heated in an oven producing a beam of strontium atoms that move out of the oven and are cooled by a Zeeman slower. The atoms are then trapped in a three-dimensional magneto-optical trap (MOT), the center of which overlaps with the mode of an optical cavity.

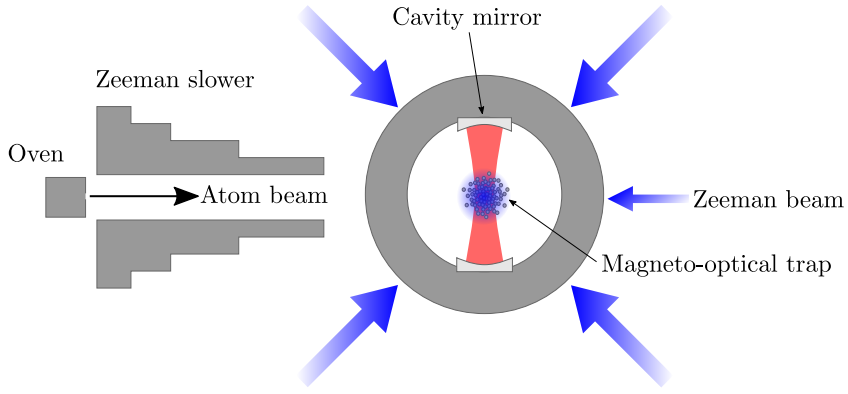

Figure 1.4: *Schematic of the of the strontium clock experiment setup. Strontium is heated in an oven and the atoms are cooled using a Zeeman slower and trapped in a three-dimensional magneto-optical trap. The center of the trap overlaps with the mode of an optical cavity.*

We can excite the atoms with a pump pulse causing them to emit a pulse of light (superradiant lasing). However, as we currently only are able to cool the atoms to a temperature of ~ 7 mK the ensemble has a Doppler broadening of a few MHz, meaning the system does not fall under the bad-cavity regime. Therefore we wish to further cool the atoms using a narrow second-stage MOT ('red MOT') using the SWAP (Saw-tooth Wave Adiabatic Passage) scheme developed by [13]. With this, we expect to reduce the Doppler broadening of the ensemble by a factor of 30 by cooling to a few µK .

1.3 Outline of the Thesis

This thesis focuses on the work done to experimentally realize a red MOT as well as experiments with the lasing pulses. In Chapter 2 the theory relevant to understand the experimental setup of the strontium clock experiment is presented. In Chapter 3 I present our current plan for the red MOT setup as well as the problems we ran into causing the red MOT to be delayed. In Chapter 4 I investigate whether we can use closely spaced pump pulses to achieve closely spaced lasing pulses. And lastly, in Chapter 5 different methods to determine the number of atoms in the MOT are investigated, as this is important for characterizing the current system as well as for the red MOT.

CHAPTER 2

Atom-Light Interactions

In this chapter I will present the theory relevant to understand the experiments described in the later chapters. In our experiments we cool and trap strontium atoms in an optical cavity. First, the energy level structure and relevant transitions of strontium are presented. The techniques to cool and trap the strontium atoms are then described and the build-up of the intracavity field is presented. To model the interaction between the atoms and the cavity field the Jaynes-Cummings model is used, and it is described here along with the strong-coupling regime.

2.1 Transitions in Strontium

In our experiments we use ^{88}Sr and the relevant energy levels for this thesis are shown in Figure 2.1 labelled using Russel-Saunders notation $^{2S+1}L_J$, where S is the total spin, L is the orbital angular momentum, and J is the total angular momentum $J = L + S$. The first few values of L 0,1,2 are also written as S, P, D.

Number	Transition	Wavelength λ	Linewidth $\gamma/2\pi$
1	$^1\mathrm{S}_0 \leftrightarrow ^1\mathrm{P}_1$	460.9 nm	32 MHz
2	$^1\mathrm{S}_0 \leftrightarrow ^3\mathrm{P}_1$	689.4 nm	7.6 kHz
3	$^3\mathrm{S}_1 \rightarrow ^3\mathrm{P}_1$	688.0 nm	5.2 MHz
4	$^3\mathrm{P}_0 \leftrightarrow ^3\mathrm{S}_1$	679.3 nm	1.75 MHz
5	$^3\mathrm{P}_2 \leftrightarrow ^3\mathrm{S}_1$	707.2 nm	8.9 MHz

Table 2.1: *Transition wavelengths and linewidths for relevant transitions of ^{88}Sr [2]. The numbers correspond to the numbers in Figure 2.1.*

Strontium is an alkaline earth metal and as such it has two valence electrons that in the ground state occupy the 5s shell resulting in a spin of $S = 0$. When one electron is excited to the 5p shell the spin can be 0 or 1, giving the singlet $^1\mathrm{P}_1$ or the triplet $^3\mathrm{P}_0$, $^3\mathrm{P}_1$, $^3\mathrm{P}_2$, respectively.

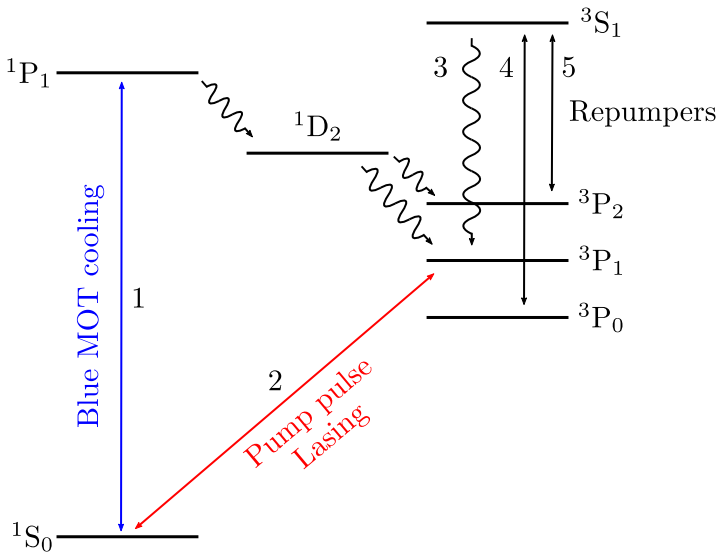

Figure 2.1: *The energy-level structure of ^{88}Sr. Full lines are transitions driven by lasers, squiggly lines represent decay channels. The wavelengths and linewidths of the transitions can be found in table 2.1.*

The two most important transitions for this thesis are the $^1S_0 \leftrightarrow ^1 P_1$ transition and the $^1S_0 \leftrightarrow ^3 P_1$ transition, which are shown in blue and red in Figure 2.1, respectively. The $^1S_0 \leftrightarrow ^1 P_1$ transition is used for cooling and trapping. It has a wavelength of $\lambda = 461$ nm and a linewidth of $\gamma/2\pi = 32$ MHz, and the latter makes it well-suited for cooling the atoms as a broad linewidth means a short lifetime which means the atoms will absorb photons often. The $^1S_0 \leftrightarrow ^3 P_1$ transition is for lasing pulses, and we want to use it for second-stage cooling. It has a wavelength of $\lambda = 689$ nm and a linewidth of $\gamma/2\pi = 7.5$ kHz. It is dipole-forbidden in the LS-coupling scheme, as it violates rule 6 in table 2.2, but can occur because of the spin-orbit coupling. In the electron's frame the proton is moving around it and this gives a magnetic field that tries to align the magnetic moment of the electron along the field. This means that L and S are no longer good quantum numbers, and and the selection rules for the LS-coupling scheme start to be violated.

1	$\Delta J = 0, \pm 1$	$(J = 0 \nleftrightarrow J' = 0)$
2	$\Delta M_J = 0, \pm 1$	$(M_J = 0 \nleftrightarrow M_{J'} = 0$ if $\Delta J = 0)$
3	Parity changes	
4	$\Delta l = \pm 1$	One electron jump
5	$\Delta L = 0, \pm 1$	$(L = 0 \nleftrightarrow L' = 0)$
6	$\Delta S = 0$	

Table 2.2: *Selection rules for electric dipole transitions in the LS-coupling scheme [3].*

As seen on Figure 2.1 atoms excited to the $^1P_1$ state can decay to the $^1D_2$ level where they can decay to $^3P_2$ and $^3P_0$. They are thus no longer getting cooled, so these are dark states. To avoid this, repumper lasers are added on the $^3P_0 \leftrightarrow {}^3S_1$ and the $^3P_2 \leftrightarrow {}^3S_1$ transitions, so atoms are pumped to $^3S_1$ and from $^3S_1$ they can decay to $^3P_1$ and subsequently to $^1S_0$.

2.2 Cooling

In our experiment we heat up solid strontium in an oven, where the sample is heated up to $T \sim 550\,°\mathrm{C}$. The strontium atoms exit the oven and travel into a vacuum chamber. Inside the oven the velocity distribution of the atoms is given by the Maxwell-Boltzmann distribution, but the distribution for the atoms in the beam going out of the oven is different. For those atoms the most probable velocity is [4]

$$v = \sqrt{\frac{3k_BT}{m}}. \tag{2.1}$$

Here k_B is the Boltzmann constant and m is the mass of an ^{88}Sr atom. From this equation the velocity of the strontium atoms coming out of the oven is calculated to be $v \sim 480\,\mathrm{m/s}$.

To work with the atoms it is necessary to localize them and thus cool them. This cooling is done with lasers and it possible because of the momentum of light. Each photon has a momentum of $\hbar k$, where wavenumber k is related to the wavelength by $k = \frac{2\pi}{\lambda}$. When a laser is shined on an atom, as in Figure 2.2, the atom can absorb a photon and will recoil from the beam. After some time the atom will spontaneously emit a photon in a random direction. Because the momentum must be conserved the change in momentum from the recoil is $\Delta p_x = -\hbar k$. When considering multiple cycles of absorption-emission the total momentum change will be in the x-direction, since the photon is reemitted in a random direction so the momentum change averages to zero. The result is a force that slows the atom down. The magnitude of this force depends on the rate at which photons are scattered, and for effective cooling we should thus use a transition with large decay rate.

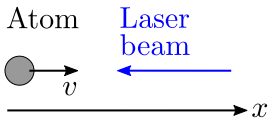

Figure 2.2: *An atom moving towards a laser beam will be cooled if the frequency of the laser is tuned slightly below atomic resonance.*

If the atom is moving towards the laser that has frequency ω_L in the laboratory frame, then in the rest frame of the atom the laser frequency is shifted

up by the Doppler effect and has frequency

$$\omega_L' = \omega_L + kv. \tag{2.2}$$

If we then tune the laser frequency to be $\omega_L = \omega_0 - kv$ and thus below the atomic resonance frequency then $\omega_L' = \omega_0$ and thus the laser will be in resonance with the atoms moving towards it.

A problem arises as the atoms are cooled because their velocity changes. As their velocity changes, the Doppler shift changes which effectively changes their resonance frequency bringing them out of resonance with the lasers. To account for this we need a force that that is velocity dependent. This can be achieved with a Zeeman slower, which will be explained in the next section.

2.2.1 Zeeman Slower

A Zeeman slower consists of a slowing beam and a solenoid with layers of decreasing length as depicted on Figure 2.3, which produces a magnetic field that varies spatially. This magnetic field changes the resonance frequency of the atoms and keeps it in resonance with the laser.

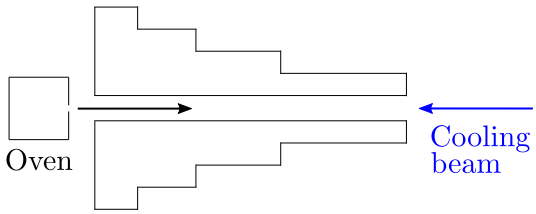

Figure 2.3: *A Zeeman slower consists of a tapered solenoid and a cooling beam. As the atoms come out of the oven they are exposed to the varying magnetic field produced by the solenoid which compensates for the change in Doppler shift as the atoms are cooled down.*

As a magnetic field B is applied to the atom its energy levels with different values of M_J are no longer degenerate, they split up. For the cooling transition this means that the level $^1\mathrm{P}_1$ splits up into 3 sublevels as seen on Figure 2.4.

The correction to the energy E_0 is given by

$$E_{ZE} = g_J \mu_B B M_J, \tag{2.3}$$

where $g_J = \frac{3}{2} + \frac{s(s+1)-l(l+1)}{2j(j+1)}$ is the Landé g-factor, with $g_J = 1$ for a singlet state, and μ_B is the Bohr magneton. This means that the Zeeman effect increases the resonance frequency by $\frac{E_{ZE}}{\hbar} = \frac{\mu_B B}{\hbar}$ and thus the magnetic field should obey the following relation

$$\omega_0 + \frac{\mu_B B}{\hbar} = \omega_L + kv, \tag{2.4}$$

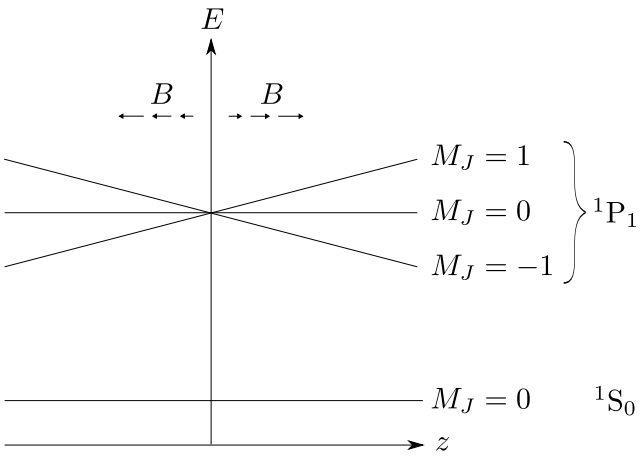

Figure 2.4: *Schematic showing the splitting of the* $^1P_1$ *sublevels due to the Zeeman effect.*

where ω_L is the angular laser frequency. This means that the atomic resonance frequency changes with position and thus the atoms are kept in resonance with the laser.

If the laser is tuned below atomic resonance (red-detuned) to account for the Doppler shift, then for $z > 0$ the $M_J = -1$ transition will be shifted closer to resonance with the laser frequency and thus the atom will absorb photons if the beam has σ^- polarization. For $z > 0$ the atom will preferentially absorb from a beam with σ^+ polarization.

2.2.2 Magneto-Optical Trap

When the atoms exit the oven and move in the z-direction they will also have small velocity components in the x- and y-directions, so they need to be cooled in all three directions. This can be achieved by having counter-propagating laser beams in all three directions as shown in Figure 2.5. An atom at rest will experience equal forces from the beams, but a moving atom will experience a net force due to the Doppler shift. The moving atom will scatter more light from the beam opposite its direction of motion if the laser is red-detuned, as explained in Section 2.2. This technique of slowing atoms is called the optical molasses technique. With the optical molasses technique the atoms can never be completely cooled because of the heating that comes from the spontaneous emission. When an atom spontaneously emits a photon it recoils and these kicks lead to a random walk in velocity space. Even though the average force from the random kicks is zero, the average force fluctuations are not zero. This gives a limit to the achievable temperature, called the Doppler cooling limit, of

$$T_D = \frac{\hbar\gamma}{2k_B}. \tag{2.5}$$

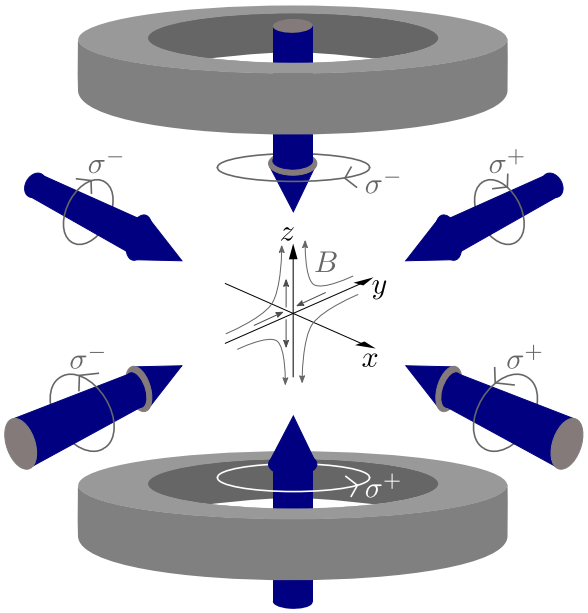

Figure 2.5: *Illustration of a magneto-optical trap (MOT). The MOT consists of six intersecting red-detuned laser beams with circular polarization and coils with currents running in opposite directions that produce a quadrupole magnetic field.*

For the blue cooling transition of ^{88}Sr this gives $T_D = 0.8\,\mathrm{mK}$.

Optical molasses can not be used to trap atoms. If atoms move away from the center there is no force to push them back. However, optical molasses in combination with a magnetic field can be used to make a trap, the so called magneto-optical trap. The magneto-optical trap (MOT) consists of six intersecting laser beams that are red-detuned with polarizations as in Figure 2.5, and a magnetic field. The magnetic field is created by two coils with current running in opposite directions and the result is a quadrupole magnetic field, which is zero in the middle and grows linearly when moving away from the middle. An atom located away from the center of the trap will experience the Zeeman effect due to the nonzero magnetic field which will cause it energy levels to shift with the shift depending on the atoms position as shown in Figure 2.4. If the atom is located at $z > 0$ then because of the Zeeman shift the $\Delta M_J = -1$ transition will be shifted closer to resonance with the laser frequency. The atom will then absorb photons from the beam with σ^- polarization and the resulting scattering force pushes it back towards the center.

For our MOT the large amount of photons from the 461 nm laser scattered means the atom cloud can be seen with the naked eye as a glowing sphere. A picture of the MOT cloud taken with a phone camera can be seen in Figure 2.6.

Our MOT has temperature of ~ 7 mK (measurements of the temperature are presented in Chapter 5). The velocity distribution of the atoms is de-

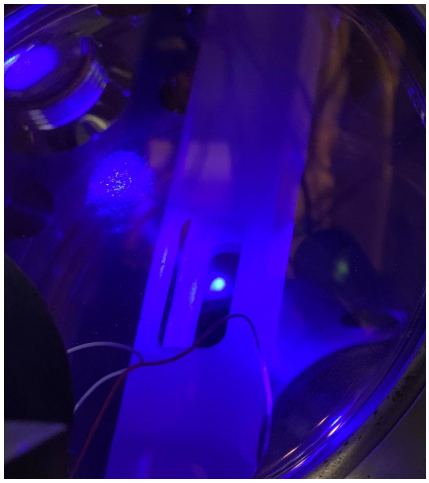

Figure 2.6: *Picture of the MOT cloud taken with a phone camera.*

scribed by the Maxwell-Boltzmann distribution, which leads to a distribution of Doppler shifts resulting in a Gaussian lineshape. This Doppler broadening can be characterized by the FWHM of the Doppler broadened linewidth, which is given by [4]

$$\nu_D = \frac{2\nu_0}{c}\sqrt{2\ln(2)\frac{k_B T}{m}}, \tag{2.6}$$

where ν_0 is the frequency of the transition and T is the temperature.

2.3 The Cavity

To enhance the interaction with the light on the narrow $^1S_0 \leftrightarrow ^3P_1$ transition the cold atoms are inside a cavity, which consists of two mirrors facing each other. We can describe the cavity using the assumptions that the mirrors are parallel and highly reflective and this type of cavity is known as a Fabry-Pérot cavity [6]. Such a cavity can be seen in Figure 2.7.

Inside the cavity a standing wave forms, as light entering the cavity will be reflected and interfere with itself. This means that the in order for the light to be resonant with the cavity, the length of the cavity has to be an integer of half wavelengths, meaning $L = q\frac{\lambda}{2}$ and thus the allowed frequencies are $\nu = \frac{qc}{2L}$. The spacing between adjacent resonance frequencies is called the free spectral range and is given by

$$FSR = \frac{c}{2L}. \tag{2.7}$$

For a lossless cavity the frequency of the light must be exactly $\frac{qc}{2L}$ or the waves will destructively interfere. This means the resonances are sharp peaks. When losses, such as finite transmission of the mirrors to be able to extract and

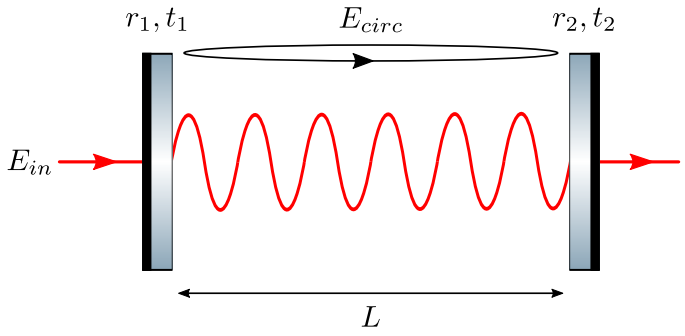

Figure 2.7: *Illustration of a Fabry-Perot cavity.*

inject light from and into the cavity, are introduced the spectrum is broadened, since the lifetime of photons inside the cavity becomes finite. The FWHM of the resonances, $\Delta\nu$, is related to the FSR by the finesse $\mathcal{F}$:

$$\mathcal{F} = \frac{FSR}{\Delta\nu} \tag{2.8}$$

As we shall see in the following section, the finesse is also a measure of the intensity amplification in the cavity.

2.3.1 The Intracavity Field

To find out how much the cavity amplifies the light in the cavity, we calculate the field circulating in the cavity, E_{circ} in Figure 2.7. Denoting the propagation phase accumulated over one round trip in the cavity as ϕ, the total electric field circulating in the cavity can be written as [10]

$$E_{circ} = t_1 E_{in} + E_{circ} r_1 r_2 e^{i\phi}, \tag{2.9}$$

The intensity of the circulating field can then be found by taking the absolute square

$$I_{circ} \propto |E_{circ}|^2 = \frac{t_1^2 I_{in}}{1 - 2r_1 r_2 \cos(\phi) + r_1^2 r_2^2}. \tag{2.10}$$

Taylor expanding the cosine to second order gives

$$I_{circ} \approx \frac{t_1^2 I_{in}}{1 + r_1^2 r_2^2 - 2r_1 r_2 (1 - \frac{1}{2}\phi^2)} = \frac{t_1^2 I_{in}}{(1 - r_1 r_2)^2 + r_1 r_2 \phi^2}. \tag{2.11}$$

From the above expression we see that the circulating intensity is a Lorentzian, and from that it is possible to find the half width at half maximum by solving $I_{circ}(\phi_{1/2}) = \frac{1}{2} I_{circ}(\phi = 0)$ for $\phi_{1/2}$. Doubling $\phi_{1/2}$ gives the full width at half maximum, $\Delta\phi$ as

$$\Delta\phi = \frac{2(1 - r_1 r_2)}{\sqrt{r_1 r_2}}. \tag{2.12}$$

The finesse is then found using the definition in Equation 2.8 and $FSR = 2\pi$

$$\mathcal{F} = \frac{FSR}{\Delta\phi} = \frac{\pi\sqrt{r_1 r_2}}{1 - r_1 r_2}. \tag{2.13}$$

Assuming that the cavity mirrors have the same transmittance $t_1 = t_2 = t$, and the same reflectivity $r_1 = r_2 = r$, and that the transmittance is much larger than any other losses we find that $r^2 + t^2 = 1$ and the intensity of the circulating field on resonance, $\phi = 0$, is

$$\frac{I_{circ}}{I_{in}} = \frac{1 - r^2}{1 - 2r^2 + r^4} = \frac{1}{1 - r^2} = \frac{\mathcal{F}}{\pi r} \tag{2.14}$$

Assuming high finesse and thus $r \sim 1$ we find that the cavity enhances the intensity by the order of the finesse. This makes the cavity a useful tool in our experiment, as it enhances the interaction between the atoms and the light.

2.4 The Jaynes-Cummings Model

The Jaynes-Cummings model describes an electromagnetic field interacting with a two-level atom. Both the field and the atom are quantized. The atom consists of ground state $|g\rangle$ and excited state $|e\rangle$ and has resonance frequency ω_0. The field is a single-mode cavity field with frequency ω and can be written as

$$\hat{\vec{E}} = \sqrt{\frac{\hbar\omega}{2\epsilon_0 V}}(\hat{a} + \hat{a}^\dagger)\vec{\epsilon}, \tag{2.15}$$

where V is the cavity volume, ϵ_0 is the vacuum permittivity and and $\vec{\epsilon}$ is the polarization vector.

The interaction Hamiltonian describing the interaction between the atom and the cavity is

$$\hat{H}_I = -\hat{\vec{d}} \cdot \hat{\vec{E}}, \tag{2.16}$$

where $\hat{\vec{d}}$ is the dipole moment operator given by

$$\hat{\vec{d}} = \langle g|\vec{d}|e\rangle \left(|g\rangle\langle e| + |e\rangle\langle g|\right) = \hat{\vec{d}}_{ge}(\hat{\sigma}_{eg} + \hat{\sigma}_{ge}). \tag{2.17}$$

Here $\hat{\vec{d}}_{ge} = \langle g|\hat{\vec{d}}|e\rangle$. $\hat{\sigma}_{eg} = |e\rangle\langle g|$ and $\hat{\sigma}_{ge} = |g\rangle\langle e|$ are the atomic transition operators. Using the expressions for $\hat{\vec{d}}$ and $\hat{\vec{E}}$ the interaction Hamiltonian becomes

$$\hat{H}_I = \hbar g(\hat{\sigma}_{eg} + \hat{\sigma}_{ge})(\hat{a} + \hat{a}^\dagger). \tag{2.18}$$

Here $g = \hat{\epsilon} \cdot d_{ge}\sqrt{\omega/(2\epsilon_0 V\hbar)}$ is the coupling constant, which describes the coupling between the atom and the field. g is described further in section 2.4.2. The full Hamiltonian, $\hat{H}_{JC}$, is created by adding $\hat{H}_I$ to the atomic Hamiltonian, $\hat{H}_{atom}$, and the field Hamiltonian, $\hat{H}_{field}$, which gives

$$\hat{H}_{JC} = \hat{H}_{atom} + \hat{H}_{field} + \hat{H}_I \tag{2.19}$$

$$= \hbar\omega_0\hat{\sigma}_{ee} + \hbar\omega\hat{a}^\dagger\hat{a} + dg(\hat{\sigma}_{eg} + \hat{\sigma}_{ge})(\hat{a} + \hat{a}^\dagger), \tag{2.20}$$

where $\hat{\sigma}_{ee} = |e\rangle\langle e|$. In the above expression for $\hat{H}_{JC}$ the terms $\hat{\sigma}_{eg}\hat{a}^\dagger$ and $\hat{\sigma}_{ge}\hat{a}$ do not conserve energy and so we make the rotating wave approximation and neglect these terms. The Jaynes-Cummings Hamiltonian is then given by

$$\hat{H}_{JC} = \hbar\omega_0\hat{\sigma}_{ee} + \hbar\omega\hat{a}^\dagger\hat{a} + \hbar g(\hat{\sigma}_{eg}\hat{a} + \hat{\sigma}_{ge}\hat{a}^\dagger). \tag{2.21}$$

2.4.1 Dressed states

The eigenstates of $\hat{H}_{JC}$ for no interaction ($\hat{H}_I = 0$) are called bare states and can be written as

$$|\psi_{1n}\rangle = |e\rangle\,|n\rangle \qquad |\psi_{2n}\rangle = |g\rangle\,|n+1\rangle\,. \tag{2.22}$$

As such the system either is in the excited state while having n photons or is in the ground state while having $n+1$ photons. The bare states can be used as a basis to obtain the matrix elements of $\hat{H}_{JC}$, $\hat{H}_{ij}^{(n)} = \langle\psi_{in}|\hat{H}_{JC}|\psi_{jn}\rangle$, which results in the following matrix

$$\mathbb{H}^{(n)} = \hbar\begin{bmatrix}\omega_0 + \omega n & g\sqrt{n+1} \\ g\sqrt{n+1} & \omega(n+1)\end{bmatrix}, \tag{2.23}$$

The eigenenergies of $\mathbb{H}^{(n)}$ are

$$E_\pm(n) = \hbar\left(n\omega + \omega_0 + \frac{\Delta}{2}\right) \pm \frac{\hbar}{2}\Omega_n(\Delta), \tag{2.24}$$

where $\Delta = \omega - \omega_0$ is the detuning, and $\Omega_n(\Delta)$ is the Rabi frequency, which is given by

$$\Omega_n(\Delta) = \sqrt{\Delta^2 + 4g^2(n+1)}. \tag{2.25}$$

The eigenstates, $|\pm, n\rangle$, associated with the two eigenenergies, $E_\pm$, are called the dressed states. The bare states, ψ_{1n} and ψ_{2n}, are split by $\hbar\omega - \hbar\omega_0 = \hbar\Delta$ and are thus degenerate for zero detuning. As depicted in Figure 2.8 the bare state pairs are separated by $\hbar\omega$ as for each pair the system contains another photon.

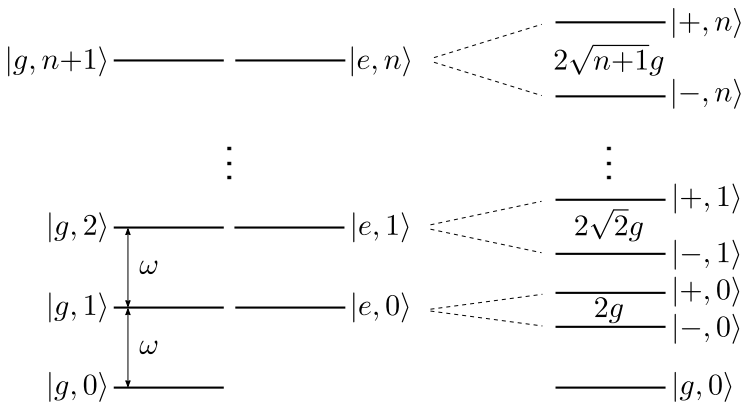

Figure 2.8: *In the Jaynes-Cummings model the bare states, $|e\rangle\,|n\rangle$ and $|g\rangle\,|n+1\rangle$, which are degenerate for zero detuning, split up into the dressed states, $|\pm, n\rangle$.*

The dressed states are non-degenerate even for zero detuning, where they are split by the frequency $\Omega_n(\Delta) = 2g\sqrt{n+1}$. As seen from Eq. 2.25 the dressed states are split even for 0 photons in the cavity field. This effect is called the vacuum-Rabi splitting. This means that when probing the coupled atom-cavity system two resonances will be present as can be seen in Figure 2.9. The vacuum Rabi splitting for zero detuning is $2g$, however for N atoms it is $2g\sqrt{N}$, and so it is easier to observe for a higher number of atoms.

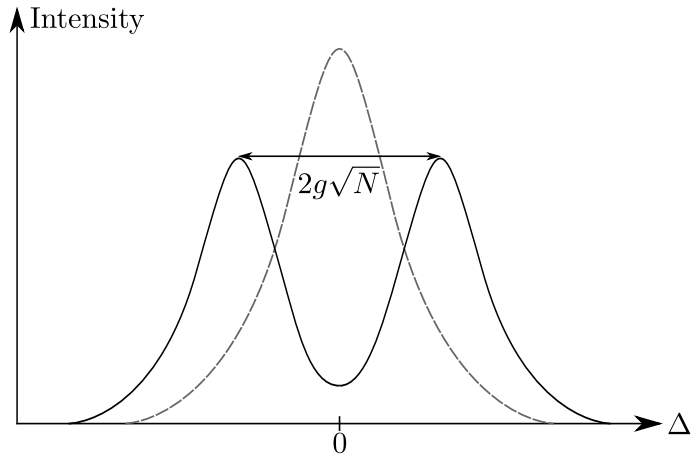

Figure 2.9: *When atoms are present in the cavity, the cavity transmission will split into two peaks seperated by $2g\sqrt{N}$.*

This splitting of the modes is not an exclusively quantum phenomenon, but also appears in coupled oscillators, where the frequencies of the coupled modes split as in the quantum case. Therefore the splitting is also referred to as normal-mode splitting.

2.4.2 Atom-cavity Coupling and the Strong Coupling Regime

The atom-cavity coupling factor g in Equation 2.18 is given by [9]:

$$g_0 = -\hat{\epsilon} \cdot d_{ge} \sqrt{\frac{\omega}{2\epsilon_0 V \hbar}}, \tag{2.26}$$

where $d_{ge} = \langle g|d|e\rangle$ is the dipole matrix element and V is the cavity mode volume. The cavity mode volume can be estimated by modelling the cavity mode as a standing-wave Gaussian mode and integrating over the length which gives $V = \pi w_c^2 L/4$, where L is the length of the cavity and w_c is the cavity waist radius. The dipole matrix element is related to the spontaneous emission rate by $\gamma = \omega_0^3 d_{ge}^2/(3\pi\epsilon_0\hbar c^3)$, and using this relation as well as the expression for V we find

$$g_0 = \sqrt{\frac{6c^3\gamma\omega_c}{w_c^2 L \omega_0^3}}, \tag{2.27}$$

where ω_c is the cavity resonance frequency. Taking the cavity mode into account, the atom will only see this coupling when it is in an antinode and in the middle of the Gaussian mode. Therefore we model the coupling as a maximal coupling multiplied by a standing wave and a Gaussian

$$g = g_0 \cdot \sin\left(\frac{\omega_c z}{c}\right) \cdot \exp\left(-\frac{x^2+y^2}{w_c^2}\right). \tag{2.28}$$

Together with κ and γ the coupling defines the characteristic time scales of the system. The Jaynes-Cummings model describes the system well when the system is in the strong coupling regime where $g \gg \kappa, \gamma$. This means that the dynamics of the system are not significantly affected by dissipation and thus that the system retains coherence. Or in other words, a photon emitted into the cavity mode is reabsorbed by the atom faster than it is lost. For an ensemble of N atoms the condition for strong coupling is $\sqrt{N}g \gg \kappa, \gamma$, so a larger N means strong coupling will be easier to obtain in the system.

CHAPTER 3

Towards a Red MOT

In this chapter I will explain the motivation for building a red MOT and present the setup as well as explaining the difficulties we ran into with regards to switching off the magnetic field.

We wish to make a MOT on the narrow $^1S_0 \leftrightarrow ^3P_1$ transition, which would lead to colder atoms, as that transition has a Doppler temperature only of 0.18 µK. The red MOT will be a second-stage MOT, such that we use the blue MOT first, because the red MOT cannot capture hotter atoms before they have been cooled by the blue MOT to ~ 5 mK. With a red MOT that relies on a mechanism where the MOT beam frequencies are swept in a saw-tooth pattern temperatures of 10 µK have been achieved [11]. With a temperature of this magnitude the Doppler broadening of the $^1S_0 \leftrightarrow ^3P_1$ transition, which is a few MHz for the current blue MOT, would be reduced by a factor of ~ 20, thus bringing the system deeper into the bad-cavity regime. Other improvements include increased coupling to the cavity and better pumping of the atoms.

3.1 SWAP MOT

We wish to make a so-called Saw-tooth Wave Adiabatic Passage (SWAP) MOT as in [13] using the 689 nm $^1S_0 \leftrightarrow ^3P_1$ transition. A SWAP MOT is similar to a regular MOT, except that the laser frequency is swept across atomic resonance in a saw-tooth patteren, as seen in Figure 3.1a. The atoms are illuminated by 3 pairs of counter-propagating beams with opposite circular polarization. If the atoms move away from zero magnetic field, they are exposed to a magnetic field gradient and their Zeeman levels are shifted, as shown for the $^1S_0 \leftrightarrow ^3P_1$ transition in Figure 3.1b. Because of the Zeeman shift, the transition from the ground state to one of the shifted levels can be made with one of the MOT lasers. As the lasers are swept upward in frequency, the level that is shifted downwards will be brought into resonance first, meaning that the population is transferred to this state. When the other level is brought into resonance the atoms cannot absorb more photons, because of the long lifetime of the $^3P_1$

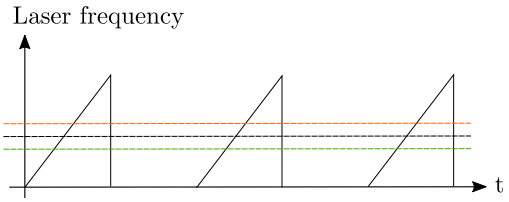

(a) *In a SWAP MOT the laser frequency is swept in a saw-tooth pattern over the frequency of the excited states. The dashed lines correspond to the Zeeman sublevels as depicted in Figure 3.1b.*

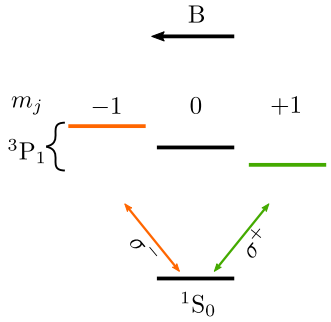

(b) *For the $^1S_0 \leftrightarrow ^3P_1$ transition in ^{88}Sr a magnetic field will cause the m_j sublevels of $^3P_1$ to split.*

Figure 3.1: *Illustrations of mechanisms used to create a SWAP MOT.*

level. Assuming that the rest of the sweep is long enough for the atoms to decay back to $^1S_0$ before the next sweep starts, a given atom will absorb more photons from one beam than the other. This leads to a force on the atom that depends on the magnetic field and thus the atomic position. This means we can use the $^1S_0 \leftrightarrow ^3P_1$ transition to trap the ^{88}Sr atoms.

An advantage of using a SWAP MOT is that the sweeping of the frequency means it is possible to address atoms with a larger range of velocities, thus making it possible to capture more atoms.

3.1.1 Adiabatic Transfer

The adiabatic part of the SWAP MOT can be understood by looking at the dressed state picture. Dressed states were introduced in section 2.4.1 in reference to the Jaynes-Cummings model. In a frame rotating at the frequency of the field the Hamiltonian is [9]

$$H = -\hbar\Delta\hat{\sigma}_{ee} + \frac{\hbar\Omega}{2}(\hat{\sigma}_{eg} + \hat{\sigma}_{ge}). \tag{3.1}$$

The Eigenvalues of this Hamiltonian gives the dressed state energies, which are

$$E_\pm = \hbar\left(-\frac{\Delta}{2} \pm \frac{\tilde{\Omega}}{2}\right), \tag{3.2}$$

where $\tilde{\Omega} = \sqrt{\Omega^2 + \Delta^2}$ is the generalized Rabi frequency. When plotting the bare and the dressed states as in Figure 3.2 we see that the energies of the bare states, 0 and $-\hbar\Delta$, cross at zero detuning, $\Delta = 0$. For the dressed states, the coupling to the field makes an avoided crossing, and thus they are no longer degenerate at zero detuning. Starting with an atom in the ground state and the laser frequency at large negative detuning, then as the laser frequency is

swept over atomic resonance and as we move to the right on the plot following the bottom branch, the atom will be transferred to the excited state. The condition for the sweep to follow the bottom line is that the space between the branches is large enough compared to the rate of the frequency sweep, $\Omega^2 \gg d\Delta/dt$.

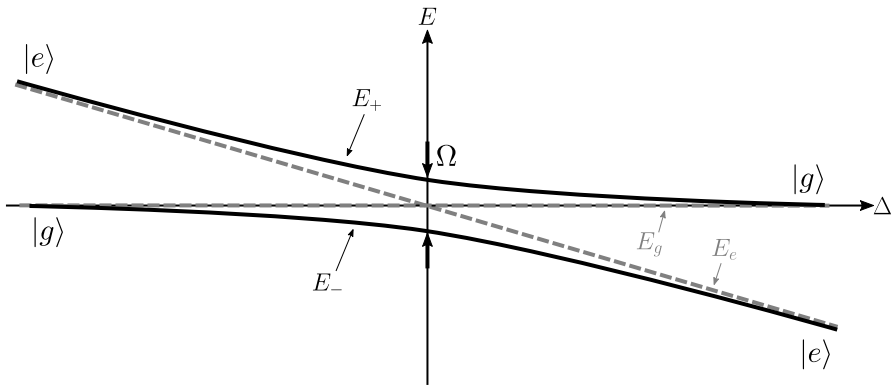

Figure 3.2: *In the Jaynes-Cummings model the bare states have energy $E_g = 0$ and $E_e = -\hbar\Delta$. When turning on the coupling between the atom and the cavity field an avoided crossing in the energy level structure appears. Adiabatic transfer means we follow the bottom branch.*

3.2 Setup for the Red MOT

The setup for the red MOT is shown in Figure 3.3. A stable clock laser locked to a cavity of finesse $\mathcal{F} \approx 8000$ is used to inject slave diode 1 by sending a weak beam of a few mW which has the correct frequency into the diode. Light from slave diode 1 is then used to inject slave diode 2. We use a tapered amplifier to amplify the light, and optical isolators are used to protect the slave diodes and the tapered amplifers from back reflections. The pump AOM seperates the beam used for the red MOT and the beam used for the pump pulse. When the pump AOM is off, the $n = 0$ order goes through another AOM used to switch the red MOT on and off. The switch AOM uses the $n = +1$ order, and we use a pinhole to block the $n = 0$ order. The $n = +1$ order from the switch AOM goes into the sweep AOM, which is used to sweep the frequency. From the sweep AOM the $n = -1$ first order is selected and the $n = 0$ order is blocked using a pinhole. A lens focuses the beam from the sweep AOM into a mirror, a so-called cat's eye configuration. The sweep AOM is a double pass configuration, where the $n = -1$ is reflected back through the AOM, so that the alignment is less sensitive to variations in diffraction angle caused by sweeping the frequency. From the sweep AOM the light goes through a PBS that divides the light into two beams, one for the xy MOT beams and one for the z beams. For the z beam the blue and the red beams are combined using

a short pass dichroic mirror, which allow for the blue beam to be transmitted and the red beam to be reflected. An achromatic $\lambda/4$ plate is used to make the polarization circular. For the *xy* beams the light is coupled into a fiber. A long pass dichroic mirror, which transmits the red light and reflects the blue light is used to combine the red and the blue light and an achromatic $\lambda/4$-plate is again used to make the polarization circular.

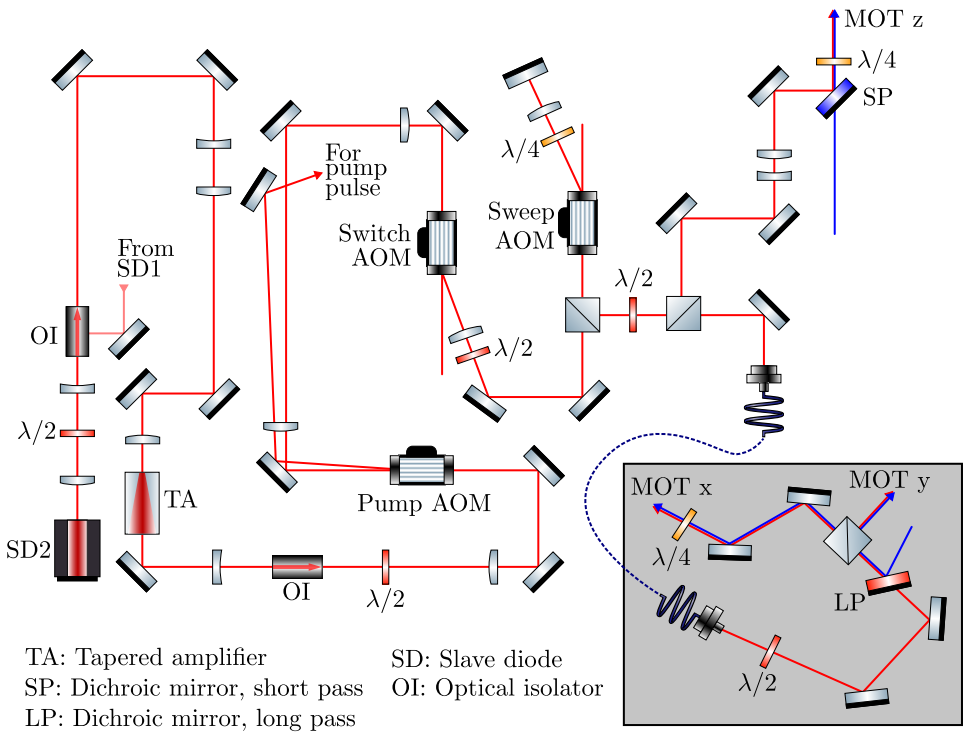

Figure 3.3: *The experimental setup for the red MOT beams. The figure is made using an Inkscape library made by Alexander Franzen.*

3.2.1 AOM frequencies

In [13] the red MOT beams are swept by ~ 7 MHz every 50 µs. In our experiment the clock laser is detuned by +40 MHz from the $^1S_0 \leftrightarrow ^3P_1$ transition. When the pump AOM is on the light passing through it is shifted by -40 MHz, bringing it into resonance with the atoms. The red MOT beams are not affected by the pump AOM, as they come from the 0th order. The switch AOM has a frequency of +120 MHz, which means that if the double-pass sweep AOM a frequency of 80-81 MHz at the end of the sweep the light will end up being just below resonance of the $^1S_0 \leftrightarrow ^3P_1$ transition. The frequency of the sweep AOM is varied using an arbitrary waveform generator that generates the signal shown in Figure 3.1a.

3.3 Switching of the Magnetic Field

When switching from the blue 461 nm MOT to the red 689 nm MOT, we would like to capture as many atoms from the blue MOT as possible. The capture radius of the MOT is defined as the distance from the center where the detuning of the MOT beams, equals the Zeeman shift

$$\Delta_{MOT} = \kappa \frac{dB}{dz} z, \tag{3.3}$$

where $\kappa = \frac{g_J \mu_B}{\hbar}$. Comparing the blue and the red MOT, the red MOT uses a smaller detuning for effective cooling. A MOT beam detuning of $\Delta_{MOT} = \Gamma/2$ gives the fastest damping, but larger detunings give larger capture velocities [15], so it is beneficial for us to use a final detuning of a few hundred kHz for the red MOT, compared to - 41 MHz for the blue MOT. In addition to the smaller detuning, the Zeeman shift for the red transition is also larger $\kappa/2\pi = 2.1\,\text{MHz}$ compared to $\kappa/2\pi = 1.4\,\text{MHz}$ for the blue transition, leading to a smaller gradient needed.

For the red MOT we need a magnetic field gradient of a few G/cm [11]. To quantize the needed reduction of the magnetic field gradient, we want to estimate the gradient we currently use for the blue MOT. This is done by measuring the magnetic field with a Gaussmeter probe above the top window of the vacuum chamber along the vertical axis, and results are seen in Figure 3.4. For the blue MOT we normally use a current of 50-60 A. However, the Gaussmeter saturates at 5 A, so the measurements were performed at a current of 5 A, and then upscaled due to the linearity between the current and the magnetic field strength. The background field, shown in Figure 3.4a was measured with the no current running through the coils.

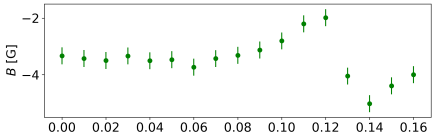

(a) *The background field, measured with no current running through the coils.*

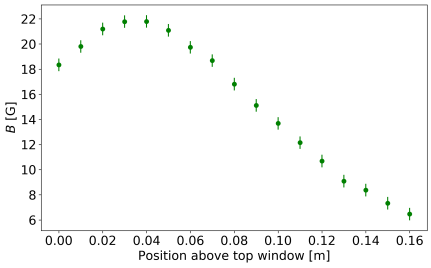

(b) *Magnetic field with a current of* $I = 5\,\text{A}$ *running through the top and bottom coil. The background, plotted in Figure 3.4a, has been subtracted from each data point.*

Figure 3.4: *Magnetic field measurements along the vertical MOT axis with 0 being the position of the top window of the vacuum chamber.*

To find the gradient we consider the expression for the magnetic field of a current loop given by

$$B(z) = \frac{\mu_0}{2} \frac{R^2 I}{(z^2 + R^2)^{3/2}}. \tag{3.4}$$

Here μ_0 is the vacuum permeability, R is the radius of the current loop, I is the current and z is the distance along the vertical axis intersecting with the loop center. As the magnetic field for the MOT is made from two current fields, the function used to fit the data in Figure 3.4b is a sum of two current loops,

$$B_{fit}(z) = \frac{\mu_0}{2} R^2 A I \left(\frac{1}{((z + z0 - d)^2 + R^2)^{3/2}} - \frac{1}{((z + z0 + d)^2 + R^2)^{3/2}} \right). \tag{3.5}$$

In the above equation, A is to compensate for the increase in the field due to the number of turns, z_0 is the offset on z due to the distance being measured above the top window and d is the distance from $z = 0$ the coils are placed at. The fit can be seen in Figure 3.5 where z_0 has been subtracted from the fit as well as the data, so $z = 0$ corresponds to the position on the vertical axis between the two coils.

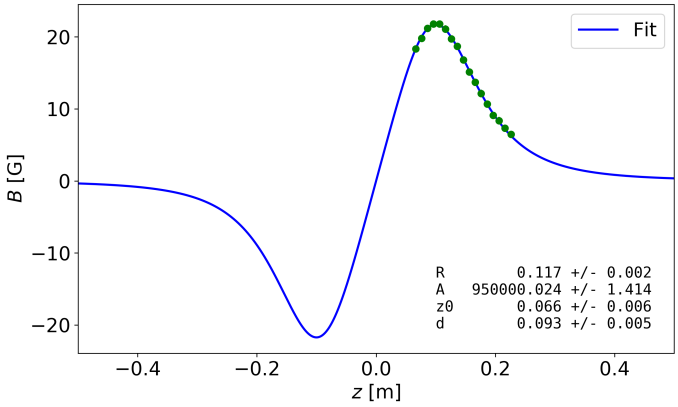

Figure 3.5: *The data in Figure 3.4b fitted to Equation 3.5. The fit parameters are shown.*

From the fit in Figure 3.5 we can find the derivative, $\frac{dB_{fit}}{dz}$, at $z = 0$ and since the expression depends on the current we can find the gradient for a current of $I = 55$ A, which results in a gradient of 33.7 G/cm. This means we need to reduce the gradient by a factor of 10 for the red MOT. The switching of the magnetic field has to be done fast, on the order of a few ms, as the thermal velocities after the blue MOT are on the order m/s, which causes the atoms to quickly move out of the capture region. This is a challenge, as the change in the magnetic flux, Φ_B, has opposite sign compared to the emf, ε, as described by Lenz's law

$$\varepsilon = -\frac{d\Phi_B}{dt}. \tag{3.6}$$

Consequently, the current produced by the emf in our coil holders, the so-called eddy currents, opposes the change in the magnetic flux. In other words, the eddy currents resist the switching off the magnetic field. Measurements of the magnetic field when switching of the coils (see Appendix A.1) revealed a decay constant of 10 ms. This meant it was necessary to design and produce a new MOT coil holder, where eddy currents are suppressed, which can be seen in Figure 3.6. The new coil holder has a gap in order to reduce the magnitude of the eddy currents in the aluminium coil holder. With the new coil holder a decay constant of 1 ms has been measured, which should make a red MOT possible. The design and production of the new holders (as well as a new vacuum chamber) delayed the red MOT and as of the date of the hand-in of this thesis a red MOT has not been made in the lab.

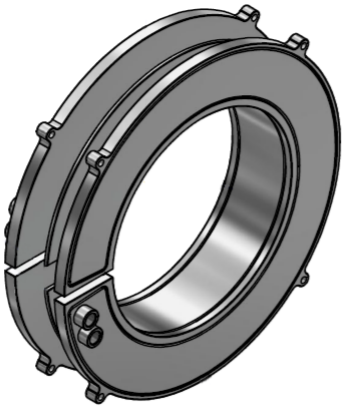

Figure 3.6: *Illustration of the new MOT coil holder with a gap to limit eddy currents.*

CHAPTER 4

Pulse Train Lasing

In this chapter we present the results of experiments where excited atoms collectively emit a pulse into the cavity mode. First we make a simulation of an atom interacting with a running-wave laser, which describes the dynamics when we use a pumping pulse to excite the atoms. Then we look at the setup for the experiment and present the result of using a single pump pulse to excite the atoms, which has been described in [12]. We investigate whether we can get many, closely spaced pulses by pumping the atoms at short intervals. To get a lasing pulse we first need to capture the atoms with the blue MOT and send a pump pulse to the atoms, and thus it is desirable to be able to get many closely spaced pulses as the dead time is then reduced.

4.1 Setup for the Pump Pulse

Atoms are cooled in a 3D MOT and the center of the trap overlaps with the center of a cavity, as illustrated in Figure 4.1. The atoms are then excited by a pump pulse incident at a 45° angle. When an atom is excited by the pump pulse it can decay spontaneously into the cavity mode, and then the light is amplified by stimulated emission from other atoms which results in a lasing pulse into the cavity mode. The light leaks out of one of the cavity mirrors and is detected on a photodetector. In these experiments the cavity is locked on resonance with the atoms using a reference field coupled into a cavity mode far off resonance (detuned by 1 FSR).

A clock laser which is stabilized to a cavity with finesse $\mathcal{F} = 8000$ is used to inject a slave diode which produces the light used for the amplifies the clock laser light, and this light is used for the probe beam. Light from the probe path is used to inject another slave diode which produces the pumping light as can be seen on Figure 3.3. This light is further amplified by a tapered amplifier and sent through an AOM, which when a radio frequency signal is applied, diffracts the light into different orders. The order that has the correct frequency to interact with the atoms is then selected. A photodetector placed on the opposite of the vacuum chamber detects the pumping power transmitted

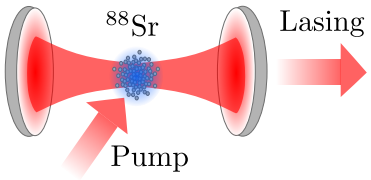

Figure 4.1: *Experimental setup for making lasing pulses.* ^{88}Sr *are cooled and trapped in a MOT and excited to the* $^3P_1$ *level by a pumping pulse causing a lasing pulse to be emitted.*

through the vacuum chamber. We expose the atoms to the pumping pulse when the MOT beams are turned off. During this time the atom cloud expands, and the atoms are lost after a few milliseconds.

4.2 Dynamics of the Pump Pulse

To trigger superradiant pulses we need to excite the atoms from the ground state to the ^{3}P$_1$ state. This can be done by shining light with the correct frequency on the atoms. To find out what happens to an atom when you shine light on it, we will look at a model consisting of a simple two-level system interacting with a running-wave laser. The two-level system consists of ground state $|g\rangle$ and excited state $|e\rangle$ and has resonance frequency ω_0. The model is semiclassical, such that the atom is quantized, but the laser is not. The Hamiltonian is

$$\hat{H} = \hbar\omega_0\hat{\sigma}_{ee} - \hat{\vec{d}}\cdot\vec{E}. \tag{4.1}$$

The first term is the energy of the atom, where the zero-point has been defined at $|g\rangle$, and the second term is the interaction of the atom with the laser, where $\hat{\vec{d}}$ is the dipole operator and $\vec{E}$ is the electric field. Making the dipole approximation and thus removing the spatial dependence of the electric field over the size of the electron cloud, the electric field becomes $\vec{E} = \vec{\epsilon}E_0\cos(\omega_L t)$, where $\vec{\epsilon}$ is the polarization vector. The dipole operator is given as $\hat{d} = \langle g|\vec{d}|e\rangle(\hat{\sigma}_{eg} + \hat{\sigma}_{ge})$. In the interaction picture with respect to $H_0 = \frac{1}{2}\hbar\omega_L\hat{\sigma}_{ee}$ the Hamiltonian is

$$\hat{H}_I = \hat{H} - \hat{H}_0 = \hbar\Delta\hat{\sigma}_{ee} + \frac{E_0}{2}\langle g|\vec{d}\cdot\vec{\epsilon}|e\rangle(\hat{\sigma}_{eg} + \hat{\sigma}_{ge}), \tag{4.2}$$

where $\Delta = \omega_0 - \omega_L$ is the detuning, with ω_L being the laser frequency. The rotating-wave approximation has been made, removing the terms which oscillate fast. We want to know how the atom responds to the light, so we want to find equations of motion for $\langle\hat{\sigma}_{ee}\rangle$ and $\langle\hat{\sigma}_{ge}\rangle$. This can be done using the interaction picture version of the master equation [7]

$$\langle \dot{\hat{A}} \rangle = \frac{i}{\hbar} \langle [\hat{H}_I, \hat{A}] \rangle + \hat{\mathcal{L}}(\hat{A}), \tag{4.3}$$

where $\hat{\mathcal{L}}$ is the Lindblad superoperator, which contains the decay rate Γ. Inserting H_I in the master equation gives

$$\langle \dot{\hat{\sigma}}_{ee} \rangle = i\frac{\Omega}{2}(\langle \hat{\sigma}_{ge} \rangle - \langle \hat{\sigma}_{eg} \rangle) - \Gamma \langle \hat{\sigma}_{ee} \rangle \tag{4.4}$$

$$\langle \dot{\hat{\sigma}}_{ge} \rangle = \left(i\Delta - \frac{\Gamma}{2} \right) \langle \hat{\sigma}_{ge} \rangle + i\frac{\Omega}{2}(\langle \hat{\sigma}_{ee} \rangle - \langle \hat{\sigma}_{gg} \rangle). \tag{4.5}$$

Here $\Omega = -\frac{\langle g|\vec{d}\cdot\vec{\epsilon}|e\rangle E_0}{\hbar}$ is the Rabi frequency. Assuming a Gaussian beam we can write the Rabi frequency as [9]

$$\Omega = \left[\frac{2\eta_0 |\langle g|d_z|e\rangle|^2 P}{\pi \hbar^2 w_0^2} \right]^{1/2}, \tag{4.6}$$

where η_0 is the impedance of free space, w_0 is the beam waist, and P is the power of the laser. The dipole matrix element is related to the decay rate by

$$|\langle g|d_z|e\rangle|^2 = \frac{3\pi\epsilon_0 \hbar c^3 \Gamma}{\omega_0^3}. \tag{4.7}$$

This can be simulated by numerically integrating Eq. 4.4 and 4.5. We use simulation parameters corresponding to the $^1\mathrm{S}_0 \leftrightarrow ^3\mathrm{P}_1$ transition and a power of $P = 50$ mW, a waist of $w_0 = 2.5$ mm, and zero detuning, $\Delta = 0$. The results for the population in the excited state, $\langle \hat{\sigma}_{ee} \rangle$ are shown in Figure 4.2.

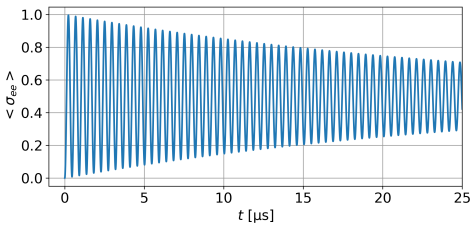

(a) *The light causes the population to make so-called Rabi-oscillations between the ground and excited state.*

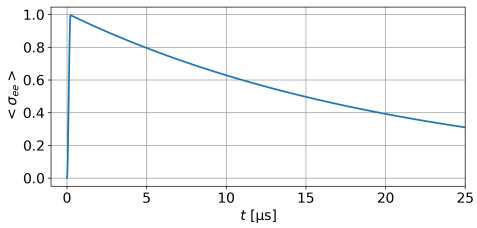

(b) *By turning off the laser when the excited state population is at the first maximum, we can make a so-called π-pulse that transfers most of the population to the excited state.*

Figure 4.2: *The excited state population $\langle \hat{\sigma}_{ee} \rangle$ found by numerically integrating Eq. 4.4 and 4.5 for the $^1\mathrm{S}_0 \leftrightarrow ^3\mathrm{P}_1$ transition with a power of $P = 50$ mW, a waist of $w_0 = 2.5$ mm, and zero detuning, $\Delta = 0$.*

In Figure 4.2a we see that the population oscillates between the ground and excited state, the so-called Rabi oscillations. Because of the decay rate the

oscillations decrease in amplitude over time, and the excited state population will eventually reach a stady state at 0.5. If we want to excite the atoms to the $^3P_1$ state, so they can emit a pulse of light, we can turn off the laser after a certain time, corresponding to a time where the excited state population is at a maximum. In this way we make a pulse that pumps the atoms to the excited state. If we choose the time corresponding to the first maximum, $t = 228$ ns, the pulse is a so-called π-pulse. In Figure 4.2b such a π-pulse has been simulated, and we see that the excited state population decays with the decay rate Γ. This simulation does not show superradiance, as we only simulate one atom interacting with a running-wave laser as opposed to multiple atoms in a cavity.

4.3 Single Lasing Pulse

An example of a single lasing pulse can be seen in Fig. 4.3 along with the pump pulse. The data shown is an average over 43 datasets selected as the pulses with a peak power larger than half the pulse with maximum peak power of 100 datasets. We see that the pulse decays faster than than the spontaneous decay time $1/\Gamma = 22\,\mu s$, which is an evidence of collective emission. The pulse does not start at 0 W, and this background is due to the reference field used to lock the cavity.

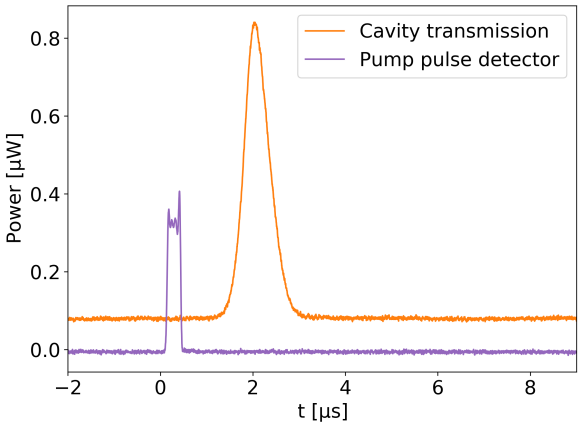

Figure 4.3: *A single lasing pulse in the cavity output. The data is an average over 43 datasets, with the 43 datasets being the ones with the largest pulses selected from 100 datasets.*

The time between the end of the pump pulse and the lasing pulse is also a characteristic of collective emission as it takes time to build up coherence in the system.

4.4 Varying the Time between the Pump Pulses

We wish to investigate whether we can we get many, closely spaced lasing pulses before the atoms leave the cavity mode after turning of the blue MOT lasers.

We use a DG535 Digital Delay/Pulse Generator to turn off the MOT lasers and start the pump pulse. The MOT lasers are turned off for 600 µs and right after the pump pulse is started. That signal is used to trigger a function/ arbitrary waveform generator (DG1062Z) that makes 5 pulses with a duration of 270 ns each (the duration was optimized for the size of the pulses). The time between the pulses is what will be varied in this experiment. The signal from the function generator is fed to the pulse AOM. We then measure the light transmission through the cavity.

We take data for 12 different pump spacings from 16 µs to 100 µs, and 100 datasets for each pump spacing. Examples of one dataset for each pump spacing can be seen on Figure 4.4, where the orange signal is the cavity transmission, the blue signal is the MOT fluorescence and the purple signal is the pump pulse detector.

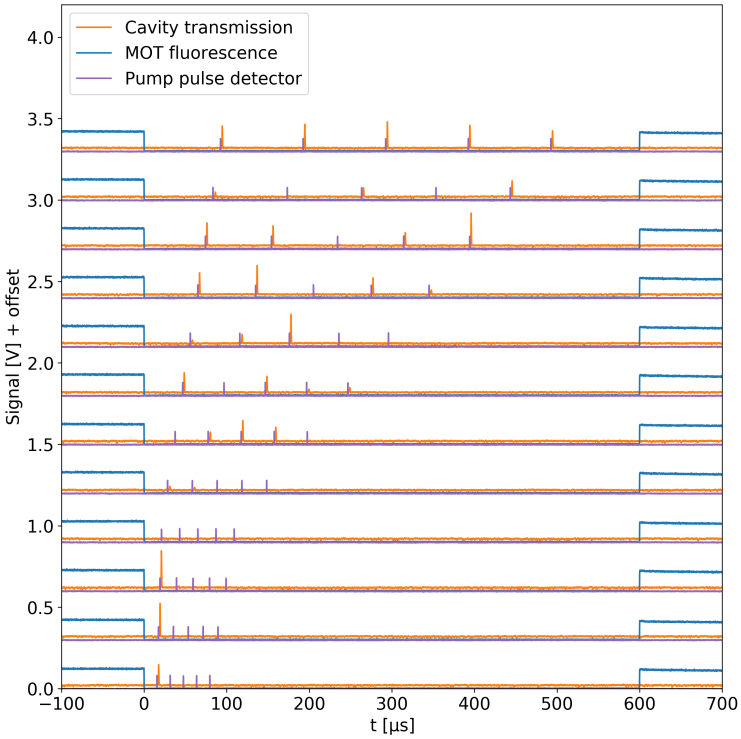

Figure 4.4: *Example of one dataset for each pump spacing. The datasets are offset on the vertical axis.*

The lasing pulses shown in Figure 4.4 are not representative of the all datasets with the same pump spacing, but show how the spacing between the pulses evolve in relation to the time the MOT is turned off. For a specific pump

spacing the lasing pulses vary quite a bit in peak power, as seen on Figure 4.5, which shows six different datasets (rows) for a pump spacing of 80 µs. These variations can be due to the fact that the MOT has to be recaptured between each measurement, and thus it slightly shifts between measurements. Considering one row separately the variations of peak size within a row are appear large as the variations between the rows. Variations within one row could be due to the pump pulses fluctuating.

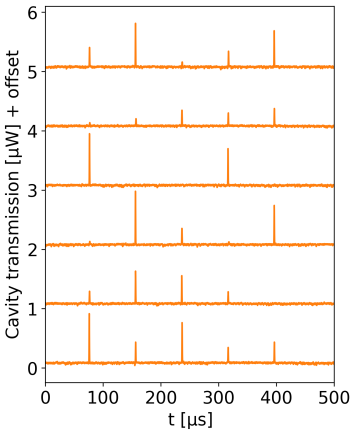

Figure 4.5: *Example of 6 datasets with 80 µs spacing, offset on the vertical axis. The pulses vary significantly in size.*

Next we look at the peak power of each of the 5 lasing pulses as a function of the time between the pump pulses, as is plotted in Figure 4.6, where pulse 1 is the first pulse after the MOT is turned off, pulse 2 is the second, and so on. The sizes are found using the function scipy.signal.find_peaks in Python. If no peak is found, where a pulse is expected, the pulse is counted as having a size of 0 W. Each point is an average over the 100 pulses.

We see that the first lasing pulse is somewhat constant in size for all pump spacings. The 2nd to 5th pulses are small, if not 0, for small pump spacings, and increase in size as the pump spacing becomes larger than the lifetime of the $^3P_1$ state, to become almost as large as the first pulse for pump spacings longer than 50 µs. That the 2nd to 5th pulses are not as intense as the first pulse for small pump spacings can be explained by the fact that not all of the excited atoms take part in the lasing (the fraction of atoms that take part in the lasing will be determined in Chapter 5). This means that after the lasing pulse is emitted, we have to wait for the rest of the atoms to decay, in order for the system to "reset". If we do not wait the next pump pulse will cause stimulated emission for some of the still exicted atoms, while exciting the atoms in the ground state that were not excited by the previous pump pulse or have had time to decay. For longer pump spacings the atoms will have had time to decay, and thus the pulses after the first pulse can be as large as the first.

To find out whether the lasing pulses are independent, we select the dataset

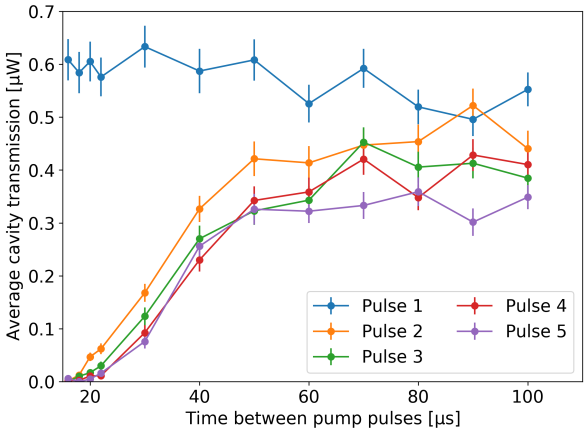

Figure 4.6: *The average size of the pulses as a function of the pump spacing. The curves each represent one of the five pulses, where pulse number 1 is the first pulse after the MOT is turned off, pulse 2 is the second, and so on.*

where the first pulse is larger than half the size of the largest pulse, and look at the sizes of the subsequent pulses. If the first pulse for a certain pump spacing is less than half the size of the largest first pulse the dataset is discarded. This removes between 50% and 60% of the data. From Figure 4.7 we see that the curve representing pulse 1 is larger than the corresponding curve in Figure 4.6, which makes sense since we selected only the largest first pulses. Pulse 2-5 in Figure 4.7 have however neither decreased nor increased in size, compared to Figure 4.6, which would indicate that they are independent from pulse 1.

Another way to confirm that the pulses are independent is to explicitly check whether pulse 2 depends on the size of pulse 1. As seen in Figure 4.8 the curve representing the peak power of pulse 2 when pulse 1 is large overlaps with the curve representing the peak power of pulse 2 when pulse 1 is small for pump spacings larger than $\sim 70\,\mu s$. For pump spacings smaller than this, the trend seems to be, that the second pulse is large when the first pulse is large. This makes sense, as the larger the lasing pulse, the more atoms have changed state, so the next pump pulse will be able to excite more atoms. However, for pump spacings larger than $70\,\mu s$ even if the first pulse is not large the atoms will have had time to decay, and thus the second pulse is independent of the first.

Thus we cannot use closely spaced pulses to reduce the dead time in our experiment and get a longer duty cycle. However, pulse 2-5 contains information about the decay time of the $^1S_0 \leftrightarrow ^3P_1$ transition, as a larger portion of the atoms have time to decay for larger pump spacings. In Figure 4.9 we plot the average of pulse 2-5 and fit an exponential function to the data.

The fitting function used is

$$f(t, a, \tau, k) = a\left(1 - e^{-\frac{t+k}{\tau}}\right), \tag{4.8}$$

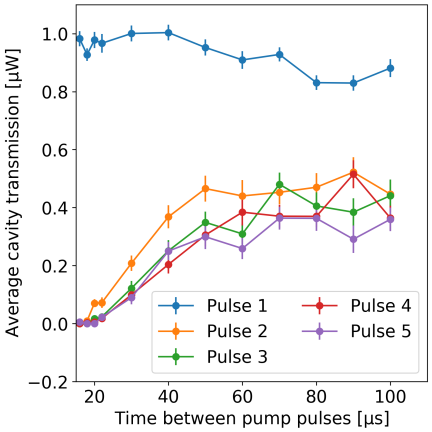

Figure 4.7: *The average size of the pulses as a function of pump spacing. Here only dataset where the first pulse is larger than half the size of the largest pulse are shown.*

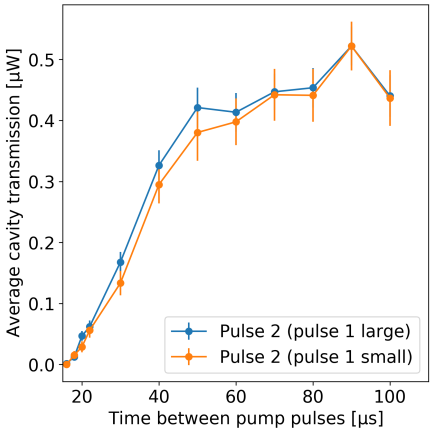

Figure 4.8: *The average peak size of the 2nd pulse as a function of pump spacing. The blue curve represents the size of the 2nd pulse where the first pulse is large, and the orange represents the size of the 2nd pulse where the first pulse is small.*

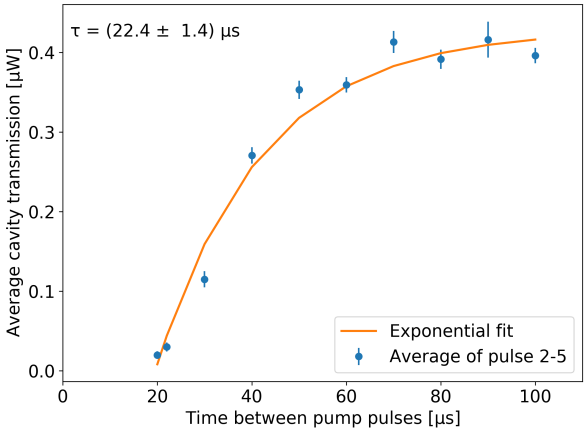

Figure 4.9: *The average size of pulse 2-5 as a function of pump spacing. From the exponential fit the decay time is found to be 22.4 ± 1.4 μs.*

where k is the offset on the time-axis and τ is the decay time. For the fitting, pump spacings with few pulses are skipped. From these data the fit time the decay is found to be $22.4 \pm 1.4\,\mu s$, which agrees well with the expected value of $20.9\,\mu s$. However, this analysis assumes that the peak height of the lasing pulses scales linearly with the population which may not be the case.

4.5 Continuous incoherent repumping

As explained in section 4.2 Rabi-oscillations make it possible to use light to excite atoms, by using a pulse with a certain length. The problem with using this method as we have seen in the previous section is that the atoms have to decay to the ground state before they are able to emit a new pulse of light. This can be solved with continuous repumping, which is the scheme shown in Figure 4.10.

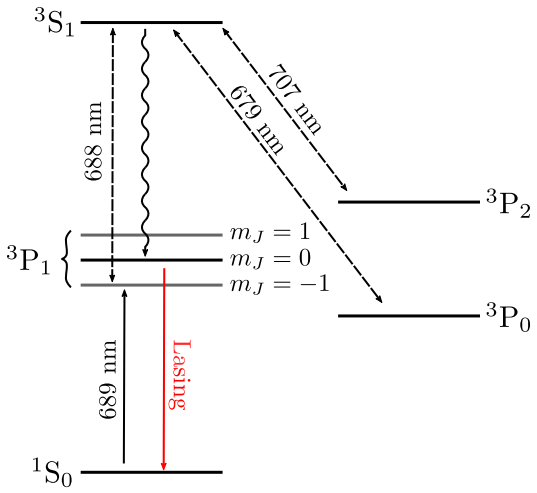

Figure 4.10: *Incoherent repumping scheme, where a 688 nm laser excites the Zeeman sublevel $m_J = -1$ of the $^3P_1$ state to the $^3S_1$ state. The 679 nm and the 707 nm laser excite the atoms that decay from $^3S_1$ to $^3P_0$ and $^3P_2$, respectively. Full lines indicate pumping/repumping, dashed lines indicate pumping/repumping as well as spontaneous emission, and wavy lines indicate spontaneous emission.*

With continuous repumping a 688 nm laser excites the Zeeman sublevel $m_J = -1$ of the $^3P_1$ state to the $^3S_1$ state. This allows spontaneous decay to the $^3P_1$ $m_J = 0$ level and can be used to create continuous lasing as atoms are continuously being excited to the $^3P_1$ state without depopulating the $m_J = 0$ state. This scheme is not currently used in our experiment, but can be implemented with a 688 nm laser and a static magnetic field. Due to the Zeeman effect caused by the magnetic field, the sublevels of $^3P_1$ split, making it possible to excite the atoms in $m_J = \pm 1$.

CHAPTER 5

Determining the Number of Atoms in the MOT

In this chapter three different methods to determine the number of atoms in the MOT are investigated. The number of atoms in the blue MOT is important to determine to characterize the efficiency of the transfer of atoms to the red MOT.

First, measurements of the normal mode splitting in the coupled atom-cavity system are presented and the method to determine the atom number is explained. Then the method of absorption imaging and determining the temperature of the MOT from time of flight measurements is described. Lastly we investigate how to find the number of atoms by counting photons in superradiant pulses.

5.1 Normal-Mode Splitting

Normal-mode splitting was presented in Section 2.4 as a signature of strong coupling in an atom-cavity system. In Figure 2.8 we saw how the energy levels of the bare atom and cavity field split when turning on the coupling between the atom and the cavity giving the so-called dressed states. This splitting can be seen in the cavity transmission as two peaks instead of one, as seen on Figure 2.9.

Equation 2.24 gives the energy of the dressed states. In that equation the detuning, $\Delta = \Delta_c = \omega_c - \omega_0$ is the detuning of the empty cavity with respect to the atomic resonance. In our experiment we vary Δ_c by varying the length of the cavity. We use a 689 nm laser to probe the coupled atom-cavity system. As we probe the transition between the ground state and the $|\pm, 0\rangle$ where one photon is shared between the cavity field and the atom we set $n = 0$ in Equation 2.24 to get an expression for the laser detuning, Δ_L

$$\Delta_L = \omega_\pm - \omega_0 = \frac{\Delta_c}{2} \pm \frac{\Omega_0}{2}, \tag{5.1}$$

where $\Omega_0(\Delta_c) = \sqrt{\Delta_c^2 + 4N_{\text{eff}}g_0^2}$ is the Rabi frequency with N_{eff} being the effective number of atoms in the cavity mode. When varying the laser detuning and the cavity detuning we can map out the avoided crossing seen in Figure 3.2, and from this we can determine the number of atoms as the splitting scales with $\sqrt{N_{\text{eff}}}$.

5.1.1 Experimental Setup

The experimental setup used to measure the normal-mode splitting is illustrated on Figure 5.1. To map out the avoided crossing we need to have a range of cavity detunings for each laser detuning (or the other way around). We can scan the laser and the cavity simultaneously. If one scan is much slower than the other we can assume one of the detunings is constant while varying the other. To do this we use two function generators. CH1 on the top one in Figure 5.1 produces a square signal that goes to a switch that controls whether the RF signal that drives the AOM is passed on. The AOM is then able to turn the MOT lasers on and off. The MOT lasers are on for 20 ms and off for 500 µs. CH2 on the top function generator is used to trigger the bottom function generator to start the laser scan. The laser and the cavity are scanned using the second function generator. The laser scan on CH1 is a triangle signal with a frequency of 1 kHz (unless otherwise stated). The output from CH1 goes to a VCO (voltage controlled oscillator) that controls the AOM for the probe laser putting the laser frequency on resonance with the atoms. The cavity is scanned slowly also with a triangle signal with a frequency of 200 mHz. This signal goes to the piezo controller where we can control the offset of the cavity scan, which goes to the cavity piezo that controls the length of the cavity.

We view the cavity transmission with an R&S RTB2004 oscilloscope. This model has a history function making it possible to save the entire cavity scan by saving 150 segments.

A single scan of the cavity transmission can be seen in Figure 5.2 and represents one cavity detuning. The orange curve is the laser scan, the blue curve is the MOT fluorescence, and the yellow curve is the cavity transmission. The laser is first scanned down in frequency, then up, meaning we see the normal mode splitting twice. The first splitting which is around 370 µs is with the MOT beams on as can be seen from the MOT fluorescence. The second and less intense splitting is at around 800 µs and is with the MOT beams on. The peaks at 200 µs and 500 µs are sidebands on the probe laser are generated by an EOM (elecro-optic modulator) at ±15 MHz. These are used to calibrate the time-axis from the oscilloscope to the detuning.

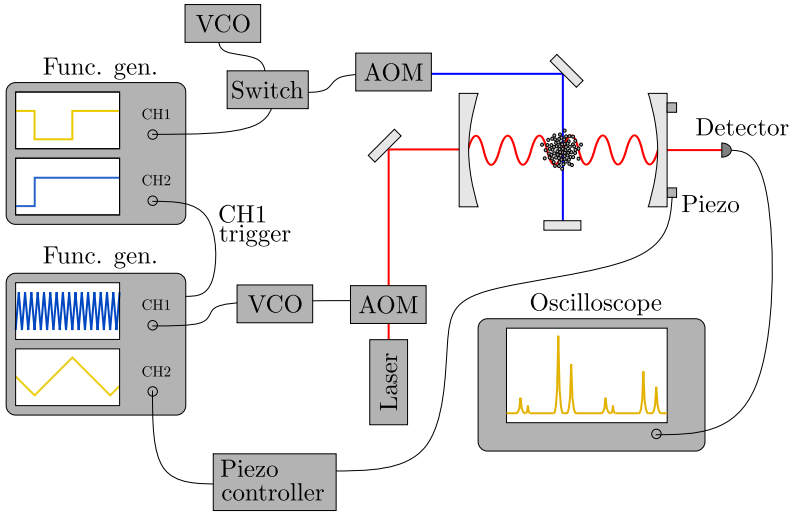

Figure 5.1: *Setup for measuring the normal-mode splitting by mapping out the avoided crossing. Two function generators are used. The top one controls the MOT beams, and the bottom one scans the laser and the cavity.*

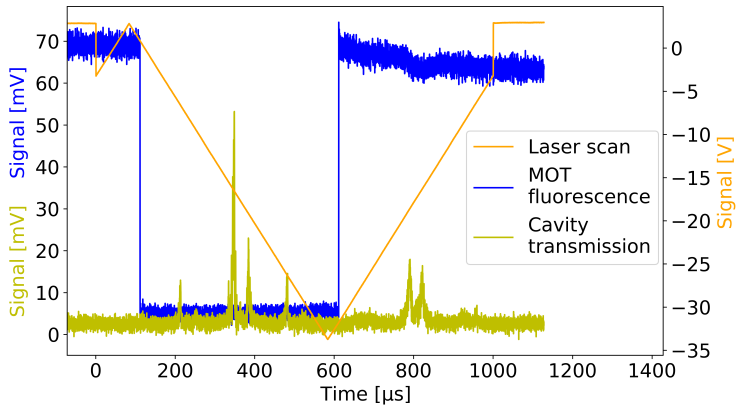

Figure 5.2: *Data for a single laser scan. The blue curve is the MOT fluorescence, the orange curve is the laser scan, and the yellow curve is the cavity transmission.*

5.1.2 Results

We plot all 150 segments on a color plot as seen in Figure 5.3, which constitutes an entire cavity scan. We have zoomed in on the time axis, so we only look at the data where the MOT beams are turned off. The transmission intensity is indicated by the color scale. We see the normal mode splitting for the middle laser scans (around scan number 75) and we see it for both the center peak and the sidebands.

We can, alternatively, switch CH1 and CH2 on the bottom function gen-

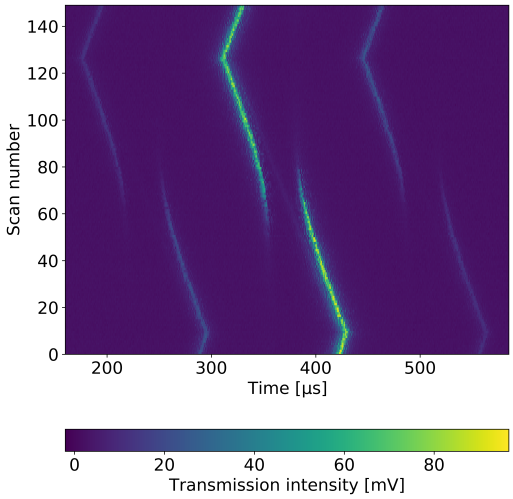

Figure 5.3: *Cavity transmission showing normal-mode splitting. For this data the laser was scanned with a frequency of 1 kHz and the cavity frequency of 200 mHz, meaning the cavity frequency will be approximately constant for one laser scan. The axis with "scan number" corresponds to the cavity axis, and the time axis corresponds to the laser axis.*

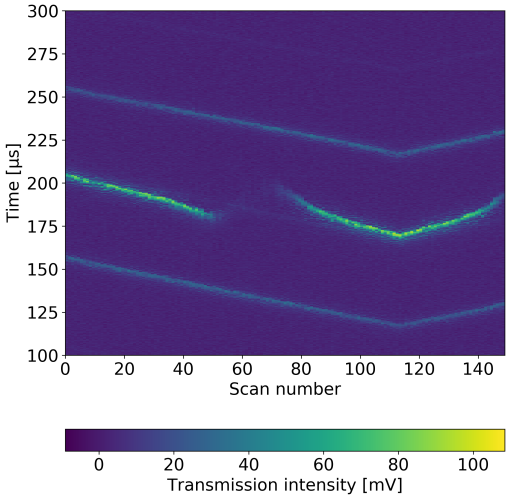

Figure 5.4: *Cavity transmission showing normal-mode splitting. For this data the cavity was scanned with a frequency of 1 kHz and the laser was scanned frequency of 200 mHz. The axis with "scan number" corresponds to the laser axis, and the time axis corresponds to the cavity axis. The normal-mode splitting is assymetrical due to the fast scanning of the cavity piezo.*

erator on Figure 5.1, so we scan the laser slowly and the cavity fast, and the result is seen on Figure 5.4. We see that the splitting is asymmetrical, which is contrary to our expectation. If the cavity piezo is scanned to fast it will exhibit non-linear behavior, which could explain the asymmetry. For quantitative analysis we therefore choose to look mainly at the "cavity slow/laser fast" scanning method. In Figure 5.4 we do not see splitting in the sidebands as the laser scan is not wide enough (see Appendix A.2).

On both Figure 5.3 and 5.4 we see a small component of the cavity transmission following the empty cavity resonance and thus not participating in the splitting. This could be due to saturation of the transition, meaning that some of light does not interact with the atoms.

Calibration of Axes

To find the number of atoms we would like to fit Equation 5.1 to the data. In order to do this the axes on Figure 5.3 are converted to cavity detuning (vertical) and laser detuning (horizontal). This is possible since we know the sidebands are at $\pm$ 15 MHz with respect to the carrier peak. To calibrate the

axes we consider two scans: The middle scan and the end scan as illustrated in Figure 5.5, where we have zoomed in onto a single cavity scan.

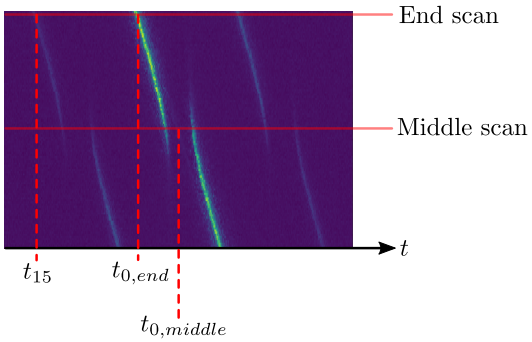

Figure 5.5: *To calibrate the axes we consider the middle laser scan and the end laser scan. We find the values of* t_{15}, $t_{0,end}$ *and* $t_{0,middle}$ *by fitting a Lorentzian function to the cavity transmission peaks as seen in Figure 5.6. This figure uses the same colorbar as Figure 5.3.*

For the middle scan we fit a sum of two Lorentzians to the split carrier peak to find the value of t corresponding to zero laser detuning, $t_{0,middle}$, see Figure 5.6a. For the end scan we fit a sum of three Lorentzians to find the positions of the sidebands t_{15} as well as the position of the carrier peak, $t_{0,middle}$. This fit can be seen in Figure 5.6a.

The laser detuning in MHz can then be calculated from the time array, t, as

$$\frac{\Delta_L(t)}{2\pi} = \frac{t - t_{0,middle}}{t_{15} - t_{0,end}} \cdot 15\text{MHz}, \tag{5.2}$$

which gives an array of laser detunings. Asumming that the end scans do not show normal mode splitting the laser detuning will be equal to the cavity

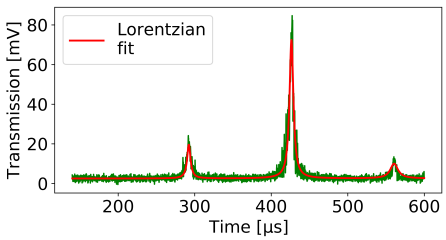

(a) *Cavity transmission for the laser scan corresponding to "end scan" in Figure 5.5. The fit function is a sum of three Lorentzians.*

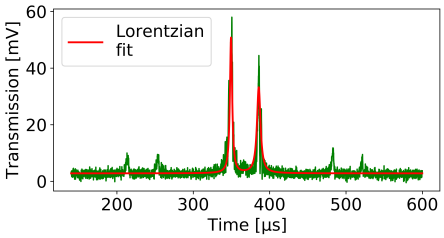

(b) *Cavity transmission for the laser scan corresponding to "middle scan" in Figure 5.5. The fit function is a sum of two Lorentzians.*

Figure 5.6: *Fits used to find the values for* t_{15}, $t_{0,end}$ *and* $t_{0,middle}$.

detuning, $\Delta_L = \Delta_c$ for the end scan. The maximal cavity detuning in MHz can then be calculated as

$$\frac{\Delta_{c,max}}{2\pi} = \frac{t_{0,end} - t_{0,middle}}{t_{15} - t_{0,end}} \cdot 15\text{MHz}. \tag{5.3}$$

This value is used to create a linear array of cavity detunings using numpy.

Varying the Probe Power

Knowing the power in the cavity is important as we want to know whether or not the atoms are saturated. The transmitted signal measured in mV can be converted to power by measuring the height (in mV) of the transmission peak without atoms by blocking the MOT lasers. This number can be converted to a power by measuring the outgoing power with a powermeter and comparing that to the intensity measured on the oscilloscope in mV. We find that 1 mV measured on the oscilloscope corresponds to a power of 1.8 nW.

The saturation intensity of the 689 nm transition can be calculated using $\gamma = 2\pi \cdot 7.5$ kHz and $\lambda = 689$ nm as [3]

$$I_{sat} = \frac{\pi hc}{3\lambda^3}\gamma = 0.03\,\frac{\text{W}}{\text{m}^2}. \tag{5.4}$$

Making the assumption that the laser beam cross section is a circle with radius equal to the cavity mode radius, $w_0 = 450\,\mu\text{m}$, we can calculate the power necessary to saturate the atoms as $P_{sat} = \pi w_0^2 I_{sat} = 19.1$ nW.

For the data shown in Figure 5.3 a power of 184 nW is used. This is the transmitted power and needs to be multiplied by $\frac{\mathcal{F}}{\pi}$ (as was demonstrated in Section 2.3) to find the intracavity power. Using $\mathcal{F} = 1260$ we find that the intracavity power is $74\,\mu\text{W}$, and thus the atoms are very saturated. This can affect the dynamics as not all photons interact with the atoms. Another effect to consider is the Doppler broadening, which leads to not all of the atoms being resonant with the probe at the same time, and thus we want to investigate the influence of saturation. Therefore we take data for lower powers, some of which can be seen in Figure 5.7. In total we take measurements for five different power levels.

For a transmitted power of 16 nW as seen in Figure 5.7c the noise compared to the signal starts to become too large making the data hard to fit. A transmitted power of 16 nW corresponds to an intracavity power of $6\,\mu\text{W}$, and thus the atoms are still saturated. We were not able to get data for a probe power that did not saturate the atoms.

Fitting

To find the number of atoms from Equation 5.1 we need to position of the carrier peak. Therefore we split the data into two parts at zero laser detuning, splitting all the laser scans in two. To each half of a scan we fit a Lorentzian

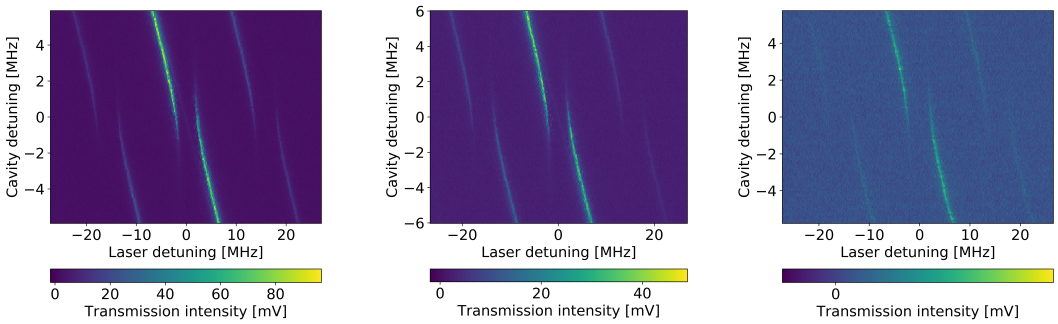

(a) *Data for a transmitted power of 184 nW.*

(b) *Data for a transmitted power of 84 nW.*

(c) *Data for a transmitted power of 16 nW.*

Figure 5.7: *Avoided crossings for three different probe powers.*

function to find the position of the carrier peak. This gives us the green points shown in Figure 5.8 for a transmitted power of 184 nW (maximum). To fit a function to these points we need to know the cavity detuning in terms of the laser detuning, which from Equation 5.1 is given as

$$\Delta_c = \frac{N_{\text{eff}} g_0^2 - \Delta_L^2}{\Delta_L}. \tag{5.5}$$

The fit for a transmitted power of 184 nW can be seen in Figure 5.8. The only fitting parameter is N_{eff}, as the coupling parameter g_0 is calculated from Equation 2.27.

In Figure 5.9 values of N_{eff} for five different powers are shown. For all five powers N_{eff} is around $7.5 \cdot 10^6$ and does not vary significantly or show any clear trend as a function of power. However for all the measured probe powers the atoms are saturated, as the lowest transmitted power corresponds to an intracavity power of 6 µW which is enough to saturate the 689 nm transition. The fact that the normal-mode splitting does not change significantly in the probe power range here means we can use a high probe power giving a good signal-to-noise ratio and derive a proxy for the total atom number. It also suggests that a more complete description of the system should include the Doppler broadening.

Also shown in Figure 5.9 are the results for N_{eff} found from the data where the MOT beams were on. This is only shown for the two largest powers as the transmission peaks measured with the MOT lasers on were much less intense, as can be seen in Figure 5.2. With the MOT beams on we find $N_{\text{eff}} \sim 5 \cdot 10^6$ atoms. Part of the decrease in atoms could be due to the 461 nm light, which excites a portion of the atoms to the $^1\text{P}_1$ state.

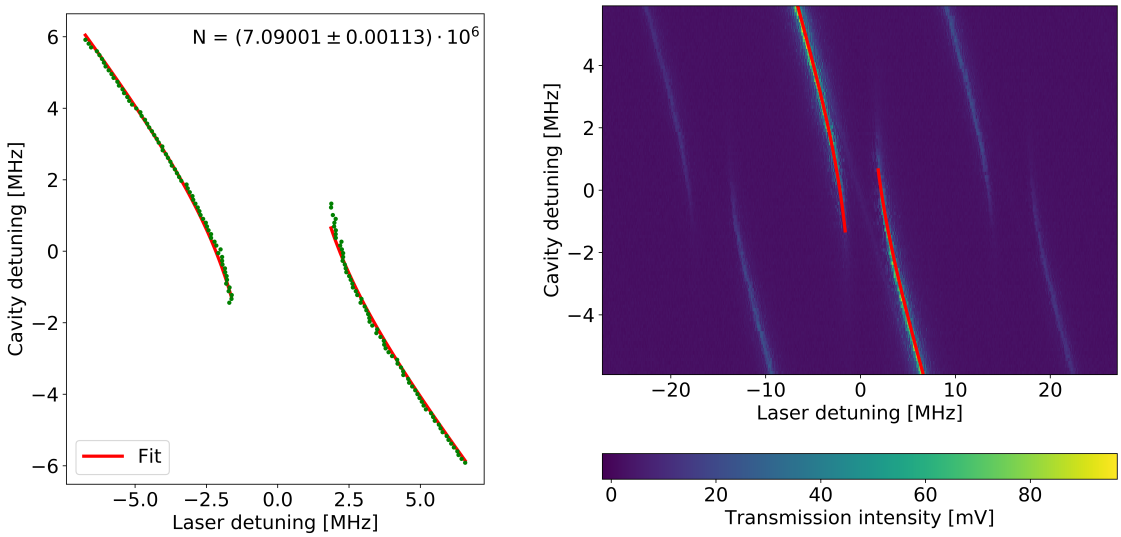

Figure 5.8: *Equation 5.5 fitted to the cavity transmission. The transmitted power is 184 nW.*

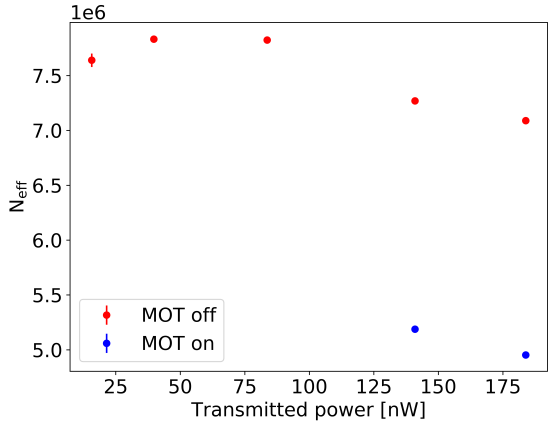

Figure 5.9: *The effective number of atoms in the cavity mode, N_{eff}, obtained by fitting Equation 5.5 to the data shown in Figure 5.7 as a function of transmitted power.*

Number of atoms in the MOT

To create a proxy for the total number of atoms in the MOT we consider the model for the coupling $g = g_0 \cdot \sin\left(\frac{\omega_c z}{c}\right) \cdot \exp\left(-\frac{x^2+y^2}{w_c^2}\right)$, described in section 2.4.2. We generate positions from Gaussian distributions (see Figure 5.10 taking into account the size of the MOT (which will be determined in the next section).

From the positions we can calculate the sine and the exponential in the

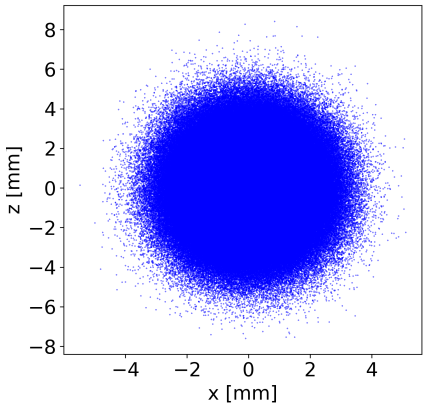

Figure 5.10: 10^6 *atom positions generated from a Gaussian distribution.*

expression for g and replace g_0 with g in the fitting routine. From this we find $N = (413.08 \pm 0.07) \cdot 10^6$ atoms in the MOT.

5.2 Absorption Imaging

Given the shortcomings of the model for the observed normal mode splitting it is very useful to employ an independent method to determine an estimate for the number of atoms in the MOT. An alternative method, already used in the group, to measure the number of atoms is absorption imaging. For this method a beam of 461 nm light with a diameter larger than the MOT cloud diameter is shined on the atoms. The atoms absorb the light and a shadow image is taken with a Flir Blackfly CCD camera (model BFLY-U3-23S6C-C). Comparing the shadow image to an image of the beam with no atoms we can find the number of atoms in the MOT cloud. The sequence used for absorption imaging can be seen in Figure 5.11. The MOT beams are on for 800 ms, and 0.2 ms after they are turned off the image light is turned on for 0.2 ms and the camera takes a picture for 1 ms (image1). 40 ms later when the MOT has dispersed, another picture is taken (image2). The image beam has a power of 0.2 mW.

An example of a shadow image can be seen in Figure 5.12a and the corresponding image without atoms in Figure 5.12b. The images shown are a mean of 6 images. 8-bit resolution is used, so each pixel can take 256 values as indicated by the colorbar.

The method used to find the number of atoms is described in [16], [17]. Beer's law for a beam on resonance with the atomic transition is given by

$$I(z) = I_0(z)e^{-OD} \Rightarrow OD = -\ln\left(\frac{I(z)}{I_0(z)}\right). \tag{5.6}$$

In this equation OD is the optical depth defined by $OD = \sigma_0 n$, where $\sigma_0 = \frac{3\lambda_0^2}{2\pi}$

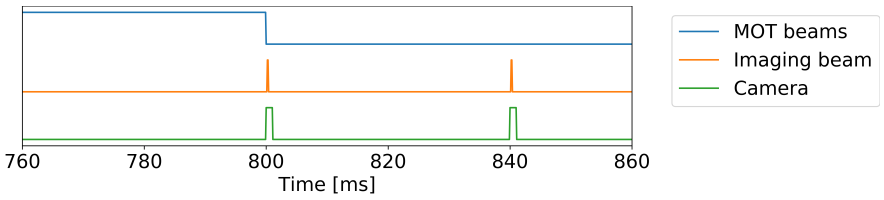

Figure 5.11: *Sequence used for absorption imaging. The MOT beams are on for 800 ms. 0.2 ms after they are turned off the image light is shined on the atoms for 0.2 ms. The camera is turned on right when the MOT beams are turned off and is on for 1 ms. After 40 ms where the MOT cloud has dispersed another picture is taken in the same way.*

and n is the column density of atoms, meaning the number of atoms within the area of one pixel. The optical depth can be found from image1 and image2 by

$$OD = \ln\left(\frac{Image2}{Image1}\right). \tag{5.7}$$

The optical depth of the MOT cloud is plotted in Figure 5.13. (note: this optical depth is not calculated from the images shown in Figure 5.12). A 3D plot of the optical depth is shown in Figure 5.14 (bottom). The number of atoms in the MOT cloud can be found by summing over the number of pixels as $N = \frac{A}{\sigma_0}\sum_{pixels} OD$, where the area is $A = (2{\cdot}5.86{\cdot}10^{-6}\text{m})^2$, since the length of one pixel is $5.86 \cdot 10^{-6}$ m and we use 2x2 binning. Instead of summing we can also integrate over the optical depth, and this can be advantageous if the cloud size is larger than the CCD chip of the camera, as integrating includes the "tails" of the cloud. We can integrate over the cloud by fitting a 2d Gaussian

$$f(x, y, B, x_0, y_0, \sigma_x, \sigma_y) = B\exp\left(-\left(\frac{(x-x_0)^2}{2\sigma_x^2} + \frac{(y-y_0)^2}{2\sigma_y^2}\right)\right) \tag{5.8}$$

where B is a constant, x_0, y_0 is the center of the cloud, and σ_x, σ_y is the width of the cloud along the x and the y direction, respectively. The fit can be seen in Figure 5.14 (top).

From the fit N is then found by

$$N = \frac{1}{\sigma_0}\int_{-\infty}^{\infty}\int_{-\infty}^{\infty} f(x, y, B, x_0, y_0, \sigma_x, \sigma_y)dxdy. \tag{5.9}$$

From 7 images taken the same day as the NMS measurements we find $N = (129.1 \pm 0.8) \cdot 10^6$.

5.2.1 Temperature of the MOT

The temperature of the MOT can be determined by absorption imaging by varying the expansion time. The temperature of the MOT is important to

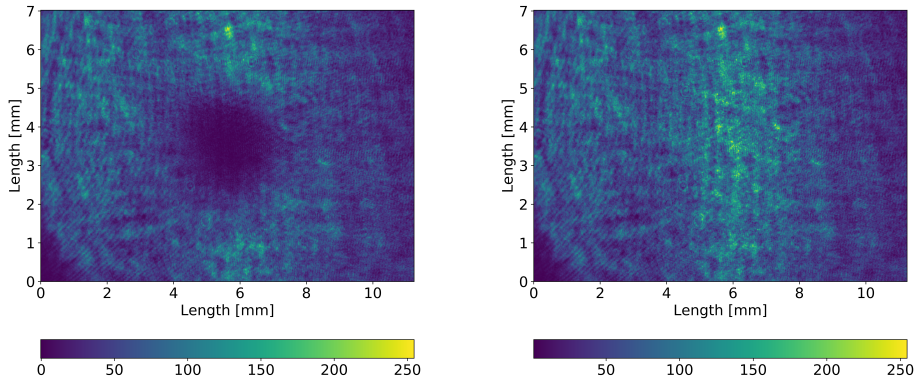

(a) *Image1: Image taken 0.2 ms after the MOT beams are turned off. The MOT cloud absorbs the image light and can be seen as a clear shadow on the image.*

(b) *Image2: Image taken 40 ms after the MOT beams have been turned off. The MOT cloud has dispersed.d*

Figure 5.12: *Images taken with the sequence in Figure 5.11. Both images are an average of 6 images.*

know in relation to the red MOT, as we are interested in significantly reducing the temperature. The temperature of the blue MOT can be found by following the same sequence in 5.11, except that we vary the delay time between the MOT beams turning off and the image beam turning off, allowing the MOT cloud to expand in between. We start with a delay of 0.2 ms and add 0.2 ms for each new expansion time for a total of 8 expansion times. The results are shown in Figure 5.15, where the optical depth is plotted. Each OD profile shown is an average over 4 consecutive measurements.

For each expansion time a 2D Gaussian (Equation 5.8) is fitted giving us a σ_x and σ_y for each expansion time. For a cloud with a Gaussian thermal equilibrium velocity distribution and Gaussian shape we expect the radii along the i'th axis to obey by the following relation [18]

$$\sigma_i(t, T, \sigma_0) = \sqrt{\frac{k_B T}{m} t^2 + \sigma_0^2}, \tag{5.10}$$

where t is the expansion time, T is the temperature, σ_0 is the width of the cloud at $t = 0$ and m is the atomic mass of ^{88}Sr. This function is fitted to the data in Figure 5.16 with the fitting parameters T and σ_0.

The temperature along the x-axis is found to be $T_x = (6.73 \pm 0.01)$ mK and the temperature along the y-axis is found to be $T_y = (7.03 \pm 0.01)$ mK. The errors on the T_x and T_y found from the fit are very small, however there could be systematic errors, for example the density distribution not being a perfect Gaussian.

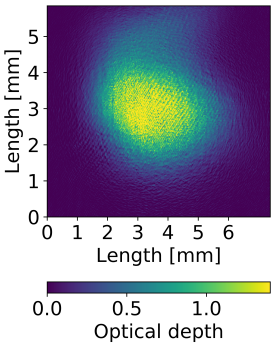

Figure 5.13: *Optical depth of the MOT cloud. Average of 7 images.*

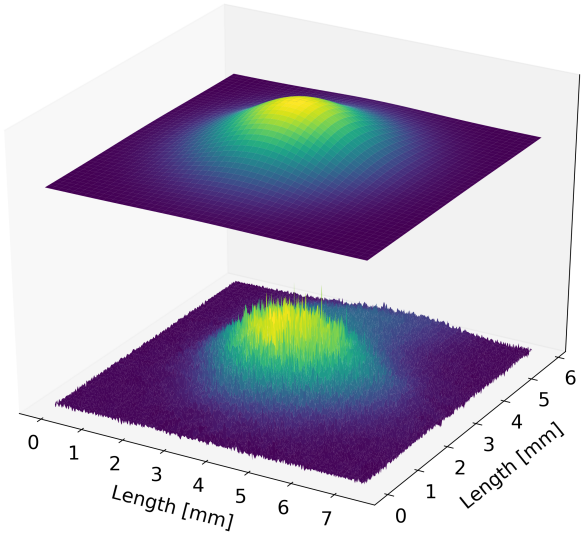

Figure 5.14: *3D plot of the MOT cloud (bottom) and fit (top).*

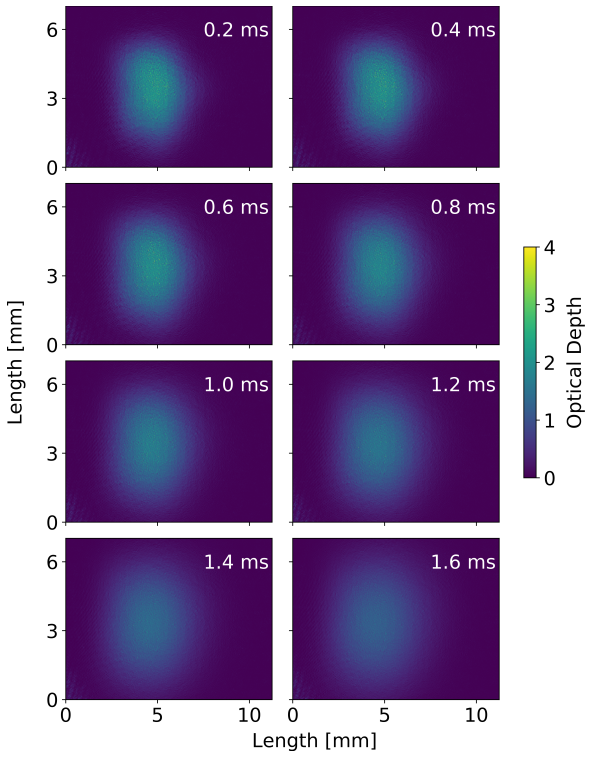

Figure 5.15: *Optical depth of the MOT cloud for 8 different expansion times.*

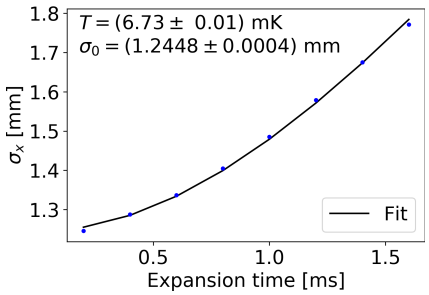

(a) *The width of the MOT cloud along the x-axis for varying expansion times.*

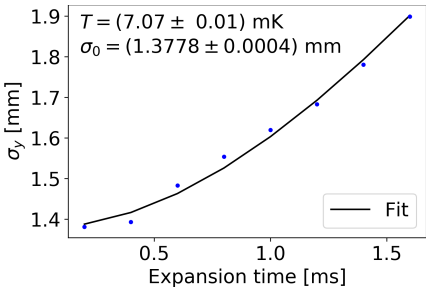

(b) *The width of the MOT cloud along the y-axis for varying expansion times.*

Figure 5.16: *σ_x and σ_y found from fitting 2D Gaussians to the OD in 5.15. The fit is Equation 5.10.*

5.3 Lasing Pulses

A third way to find the number of atoms is using the superradiant pulses described in chapter 4. We use the same setup as described in section 4.1, except the MOT lasers are turned on right after the pump pulse is turned off, leading to the lasing pulse being emitted when the MOT lasers are turned on, as seen in Figure 5.17 where one such measurement is plotted.

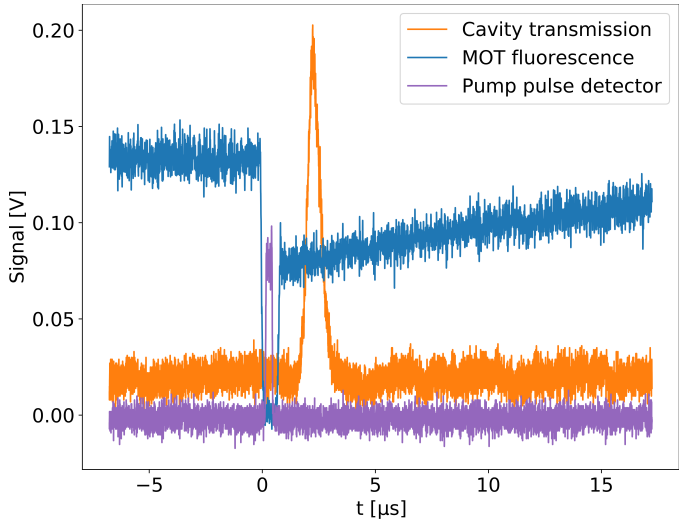

Figure 5.17: *Example of one of the 19 datasets used to find the number of atoms.*

In Figure 5.18 an average of 19 pulses is shown. From integrating the area between the cavity output and the background we can determine the energy of the pulse, E and thus the number of photons

$$n = \frac{E}{\hbar\omega} = 1.4 \cdot 10^6. \tag{5.11}$$

The number of photons emitted corresponds to the number of atoms changing state due to emitting photons during the lasing process. However, as described in chapter 4 not all atoms take part in the lasing process.

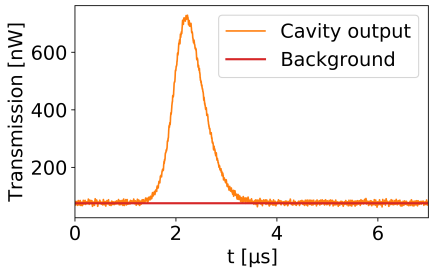

Figure 5.18: *Average of 19 lasing pulses. The energy of the pulse is found by integrating the area between the cavity output and the background.*

To determine what fraction of the total number of atoms take part in the lasing process, we can use the the MOT fluorescence, as it contains information about the population transferred between the $^1S_0$ and $^1P_1$ state. The fluorescence level when the MOT beams are on before the pumping pulse corresponds to all atoms contributing to the MOT fluorescence. When the pump beam is turned on a fraction of the atoms are excited to the $^3P_1$ level. As the MOT beams are turned on immediately after the pump pulse the fluorescence level is reduced. From the ratio of the fluorescence level the fraction of excited atoms can be determined.

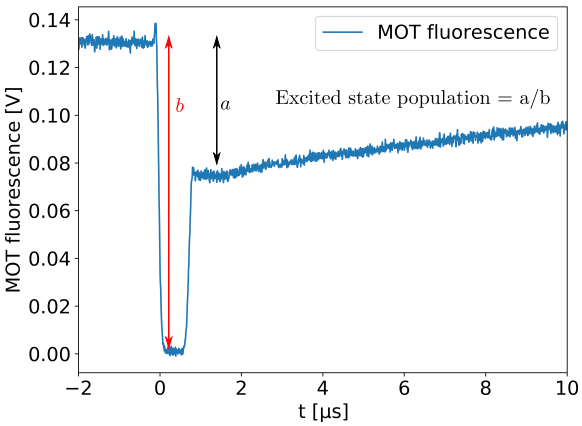

Figure 5.19: *MOT fluorescence data used to determine the excited state population.*

The excited population is shown in Figure 5.20 (blue curve). As the data is quite noisy a moving average is shown on top of the actual data. An exponential function (red curve) is fitted to the fluorescence data after the lasing pulse (green data). This exponential decay of the excited population is due to the spontaneous emission from the $^3P_1$ state. By subtracting the exponential

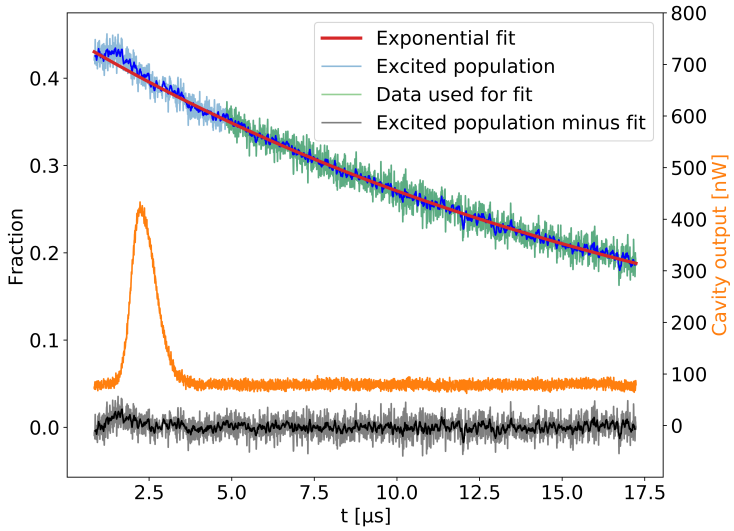

Figure 5.20: *The excited population (blue curve) with moving average plotted on top due to the noise. An exponential function (red curve) is fitted to the fluorescence data after the lasing pulse (green data). The number fraction of atoms participating in the lasing is found from the black curve which is the exponential fit subtracted from the total excited population.*

fit from the total excited population (black curve) the fraction of atoms participating in the lasing process can then be found by taking the difference in the black curve before and after the lasing pulse. This is found to be $(1.4 \pm 0.9)\%$, meaning that the number of atoms in the MOT is $N = (98 \pm 63) \cdot 10^6$. However, the fraction of atoms participating in the lasing is quite uncertain due to the noise in the data. In [19] the signal to noise ratio was improved by averaging over 1024 measurements.

5.4 Comparison of the Different Methods

In this chapter three different methods for determining the number of atoms in the MOT have been presented. The number of atoms in the MOT can vary from day to day depending on fluctuations in the power and alignment of the MOT beams. In order to compare the numbers obtained for the different methods, it is important that the measurements have been taking within a short time of each other. As the measurements with the lasing pulses were taken many months before the NMS and absorption imaging measurements, it is difficult to compare the number obtained from the lasing pulse measurements with the two others. However, the measurements of the NMS and the absorption imaging were taken on the same day, so it makes more sense to compare those two.

For the NMS measurements (for maximum power) the number of atoms in the MOT was found to be $N = (413.08 \pm 0.07) \cdot 10^6$ and for the absorption imaging measurements $N = (129.1 \pm 0.8) \cdot 10^6$, which is a significant difference, and is most likely an indication of a systematic error in the number found from the NMS measurements. The model used to determine this number does not include the Doppler broadening and saturation of the atoms, which makes it insufficient for describing our system. A more complete model would be necessary to determine the atom number precisely, but this was not possible in this thesis due to time constraints. However, we have verified that the normal-mode splitting for our system is insensitive to a range of probe powers meaning we can use it as a proxy for the total atom number.

CHAPTER 6

Conclusion

In this thesis we looked at the steps needed to experimentally realize a second-stage narrow-line SWAP MOT to cool strontium atoms to µK level. A temperature of this magnitude would reduce the Doppler broadening of the $^1S_0 \leftrightarrow ^3P_1$ linewidth by a factor of ∼30 and bring the system deeper into the bad-cavity regime. However, the fast switching of the magnetic field necessary for creating the MOT caused delay of the process as it was necessary to produce new MOT coils to limit eddy currents.

We also investigated whether we could get closely spaced superradiant lasing pulses by pumping the atoms at short intervals. This was not possible due to the need for the system to decay back to the ground state between pump pulses.

Finally we investigated different methods to determine the number of atoms in the current blue MOT. We measured the normal-mode splitting of the coupled atom-cavity system and using the Jaynes-Cummings model found the atom number to be $N = (413.08 \pm 0.07) \cdot 10^6$. The model used does not take Doppler broadening and saturation into account which is present in our system, which means that we find a large difference between this result and the result found from the method of absorption imaging which was $N = (129.1 \pm 0.8) \cdot 10^6$. However, by investigating the normal-mode splitting we found that it is insensitive to a range of probe powers meaning we can use it as a proxy for the total atom number. For the last method we found the atom number by counting photons in the lasing pulses. These measurements gave a result of $N = (98 \pm 63) \cdot 10^6$, and the large uncertainty is due to noise in the data which could be minimized by taking more measurements.

6.1 Future Prospects

The next step for the strontium clock experiment is making the red MOT and characterizing it by measuring the number of atoms and the temperature us-

ing the same methods as have been used in this thesis to characterize the blue MOT.

Inchoherent repumping of the atoms would solve the problem with the timing constraints of the pump pulses. To experimentally realize this scheme we need a 688 nm laser which is currently being set up as well as a static magnetic field to split the $^3P_1$ state, which we plan to achieve by ramping just one of the MOT coils.

To get an accurate number of atoms from the normal-mode splitting data we need a model which includes Doppler broadening and saturation of the atoms. The Doppler broadening can be experimentally studied by preparing clouds at different temperatures, which will be interesting to do in relation to the red MOT. The normal-mode splitting can also be further investigated by preparing MOT clouds with different and independently measured atom numbers.

Appendices

A.1 Decay of the Magnetic Field

Figure A.1 shows the difference magnetic field decay measured with a Gaussmeter between using the old and the new coil holder, the latter being ther one depicted in Figure 3.6. The decay constant is found from an exponential fit, and as seen in Figure A.1 the new coil holder reduces the decay time by a factor of 10.

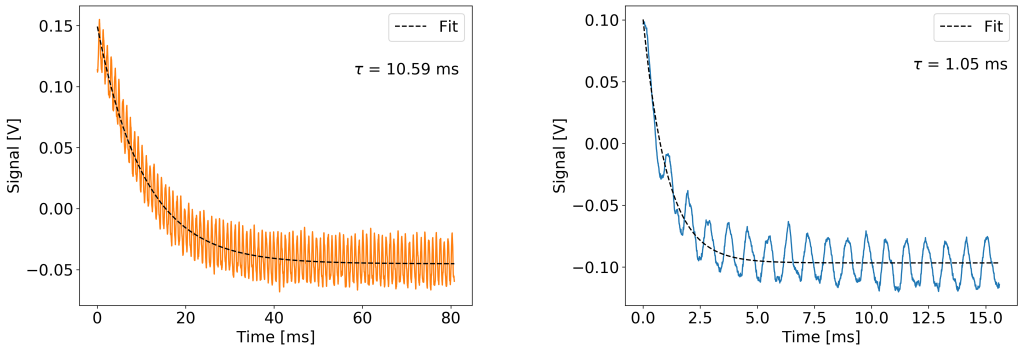

(a) *Magnetic field decay using the old coil holder.*

(b) *Magnetic field decay using the new coil holder depicted in Figure 3.6.*

Figure A.1: *The magnetic field measured with a Gaussmeter after turning of the coils.*

A.2 NMS with Fast Scanning of the Cavity

In Figure A.2 we show measurements of the normal-mode splitting for the same conditions as in Figure 5.4 except the laser scan is wider (100 mHz) making it possible to see normal-mode splitting of one of the sidebands.

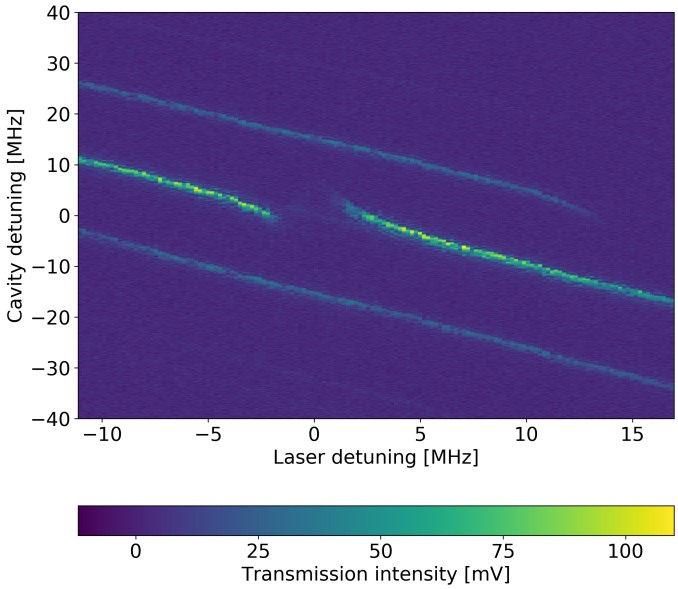

Figure A.2: *Cavity transmission showing normal-mode splitting. The cavity i scanned with a frequency of 1 kHz, and the laser was scanned with a frequency of 100 mHz.*

Bibliography

[1] C. W. Chou et al, (2010). *Frequency Comparison of Two High-Accuracy Al^+ Optical Clocks*, Phys. Rev., vol. 104, iss. 7

[2] I. Courtillot, (2003). *Première observation de la transition fortement interdite 1S0-3P0 du strontium, pour une horloge optique à atomes piégés*

[3] C. J. Foot, (2005). *Atomic Physics.* Oxford University Press.

[4] M. Fox, (2006). *Quantum Optics: An Introduction.* Oxford University Press.

[5] P. Milonni and J. Eberly, (2010). *Laser Physics.* John Wiley & Sons.

[6] B. E. A. Saleh and M. C. Teich, (1991). *Fundamentals of Photonics.* John Wiley & Sons.

[7] T. M. Barlow, R. Bennett and A. Beige, (2015). *A master equation for a two-sided optical cavity*, Journal of Modern Optics

[8] C. Gerry and P. Knight, (2008). *Introductory Quantum Optics.* Cambridge University Press.

[9] D. A. Steck. *Quantum and Atom Optics* (revision 0.13.4, 24 September 2020)

[10] H. Carstens, (2016). *Enhancement cavities for the generation of extreme ultraviolet and hard x-ray radiation*, PhD Thesis, Ludwig Maximilian University

[11] J. A. Muniz et. al, (2018). *A Robust Narrow-Line Magneto-Optical Trap using Adiabatic Transfer*

[12] S. A. Schäffer et. al, (2020). *Lasing on a narrow transition in a cold thermal strontium ensemble*, Phys. Rev. A, vol. 101, iss. 1

[13] M. A. Norcia, (2018). *New tools for precision measurement and quantum science with narrow linewidth optical transitions*, PhD Thesis, University of Colorado

[14] J. Gea-Banacloche, H. Wu, and M. Xiao, (2008). *Transmission spectrum of Doppler-broadened two-level atoms in a cavity in the strong-coupling regime*, Phys. Rev. A, vol. 78, iss. 2

[15] E. C. Cook, (2017). *Laser Cooling and Trapping of Neutral Strontium for Spectroscopic Measurements of Casimir-Polder Potentials*, PhD Thesis, University of Oregon

[16] K. Luksch, (2012). *Measurement of the Number of Atoms in a Magneto-Optical Trap Using Absorption Imaging*

[17] A. Hilliard, (2008). *Collective Rayleigh scattering in a Bose Einstein condensate*, PhD thesis, Niels Bohr Institute, University of Copenhagen

[18] P. Arora, (2012). *Measurement of Temperature of Atomic Cloud Using Time-of-Flight Technique*, MAPAN-Journal of Metrology Society of India

[19] M. Tang, (2018). *Modeling Lasing in a Thermal Strontium Ensemble*, M.Sc. Thesis, Niels Bohr Institute, University of Copenhagen